

## Chapter 2

# Problem Statement: Modification of $p_T$ Spectra in AA Collisions

Could a heavy-ion collision be described by a superposition of individual nucleon-nucleon collisions? If not, which mechanisms are responsible for a deviating behaviour? How could this deviation be quantified and how could it be related to the properties of the created matter?

Experimentally, as an entrée to the unfolding of the peculiarities of heavy ion collisions, differential analyses of particle abundances as a function of the transverse momentum ( $p_T$ ) are commonly performed. The advantage of the analysis of  $p_T$  distributions over those of longitudinal momentum  $p_L$  is given by the fact that the initial parton  $p_T$  is negligibly small as compared to  $p_L$  and thus the final  $p_T$  of the produced hadrons is predominantly created during the collision process. Therefore, the  $p_T$  spectra of the measured hadrons provide a link to the underlying processes of the reaction and the system evolution. Performing this for different collision centralities in nucleus–nucleus (AA) collisions, i.e. for different overlap areas of the colliding nuclei, the changes of the  $p_T$  distribution for different amounts of participating<sup>1</sup> or colliding<sup>2</sup> nucleons can be studied: Do the features of the medium change with the number of colliding nucleons? Is it possible that a Pb–Pb collision is similar to a pp collision if peripheral enough? These questions lead to the comparison of  $p_T$  distributions from Pb–Pb collisions to those from pp. Since the underlying theory to describe the reactions in pp at high  $p_T$  is pQCD (for the vacuum case), the  $p_T$  spectra in pp provide a reference for understanding the QCD processes embedded in a medium created in Pb–Pb collisions. A common quantitative measure of the difference of pp and Pb–Pb collisions is the nuclear modification factor

---

<sup>1</sup>Participating nucleons are those nucleons, which suffered at least one inelastic interaction.

<sup>2</sup>The number of colliding nucleons or the number of average binary collisions describes the total number of inelastic nucleon-nucleon collisions.

$$R_{AA} = \frac{1}{\sigma_{\text{INEL}}^{\text{pp}} \langle T_{AA} \rangle} \cdot \frac{(dN/dp_T)_{AA}}{(dN/dp_T)_{pp}} \quad (2.1)$$

as introduced in [1] with  $\sigma_{\text{INEL}}^{\text{pp}}$  as the total inelastic hadronic cross section in pp collisions and  $\langle T_{AA} \rangle$  as the nuclear thickness function. Since  $\sigma_{\text{INEL}}^{\text{pp}} \cdot \langle T_{AA} \rangle = \langle N_{\text{coll}} \rangle$ , the total number of binary nucleon-nucleon (NN) collisions in AA collisions, the following equation is frequently used:

$$R_{AA} = \frac{1}{\langle N_{\text{coll}} \rangle} \cdot \frac{(dN/dp_T)_{AA}}{(dN/dp_T)_{pp}}. \quad (2.2)$$

The result from pp collisions is scaled  $p_T$ -independently by the number of possible binary NN collisions in a Pb–Pb collision. A deviation of  $R_{AA}$  from unity hence reveals, that the Pb–Pb collisions are not simple super-positions of individual nucleon-nucleon collisions. It should be noted, that the assumed binary collision scaling applies only to hard processes, i.e. to processes that contribute predominately to the high- $p_T$  region [2]. At low  $p_T$ , the particle production scales with the number of participants ( $N_{\text{part}}$ ) [3], which means that only the number of nucleons taking part in the reaction are relevant but not the individual nucleon-nucleon collisions. Thus, a deviation of  $R_{AA}$  from unity at low  $p_T$  can be expected, if  $N_{\text{coll}}$  is used for the  $R_{AA}$  calculation. Alternatively,  $R_{AA}$  scaled with  $N_{\text{part}}$ , as it was performed in [4], can be studied to investigate the low  $p_T$  region and the transition to a probable  $N_{\text{coll}}$  scaling.

Typically, for hadrons, consisting of strongly interacting partons, this parameter is smaller than unity, disclosing that the medium is strongly interacting. If so, one speaks about a suppression of the particle yields as a function of  $p_T$  or centrality in Pb–Pb as compared to pp. In 1982 Bjorken already predicted such a suppression for hadrons at high  $p_T$  [5], which was later referred to as jet quenching in [6] (see Sect. 2.1). An example for  $R_{AA}$  of charged particles (mainly hadrons: pions, kaons and protons) is shown in Fig. 2.1, where the results published by the ALICE collaboration [7] are displayed. In contrast to hadrons, there is no suppression visible for electromagnetic and/or weakly interacting particles (see Fig. 2.2), such as photons,  $W^{+,-}$  and  $Z^0$  bosons respectively, which underlines the dominance of the strong interaction in the medium. Moreover, the binary collision scaling shows that their production rates are not modified by the presence of a medium.

The interpretation of the observed hadron suppression in AA collisions is that an elementary reaction between two colliding partons—including their scattering as well as their properties after the scattering and their fragmentation into hadrons—is modified by the surrounding medium. This modification could possibly be driven by

- absorption
- energy loss

in the medium, which are currently considered as the dominant effects. While the first effect would lower the  $p_T$  spectrum due to a decrease of the abundance (downward shift), the latter could cause a shift of the spectrum to lower  $p_T$  values (shift to the left) [9]. For the high  $p_T$  region, one would expect that the energy loss dominates as

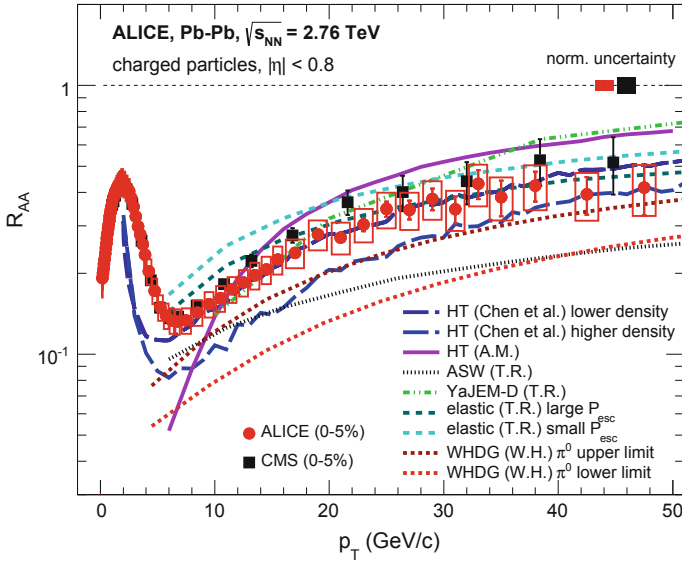


**Fig. 2.1** Nuclear modification factor  $R_{AA}$  of charged particles measured by ALICE in the most central Pb-Pb collisions (0–5 %) at  $\sqrt{s_{NN}} = 2.76$  TeV in comparison to results from CMS and different model calculations [7]

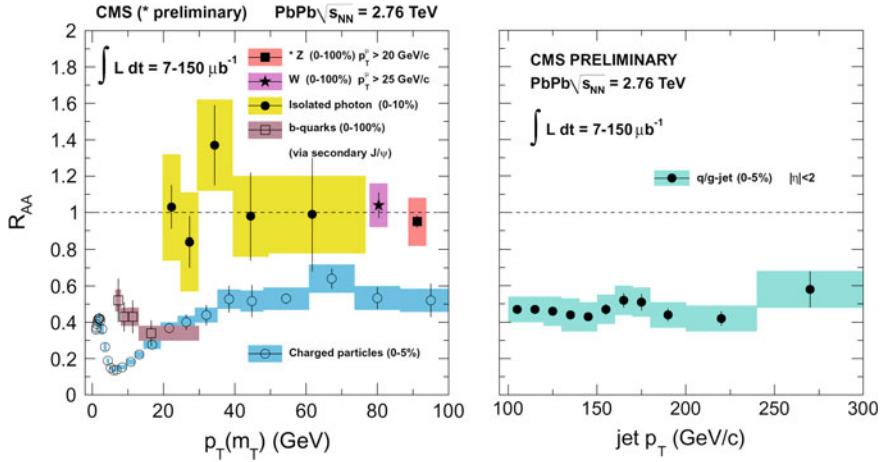


**Fig. 2.2** Nuclear modification factor  $R_{AA}$  of different particles measured by CMS [8]

a function of the length traversed by the parton in the medium, since the momentum is still large enough for escaping the medium and fragmenting outside into hadrons before being absorbed. Whether fragmentation inside the medium needs to be taken into account and if this process is modified is currently under investigation.

Two momentum regions can roughly be distinguished in the  $R_{AA}$  distribution in Fig. 2.1: the low-to-intermediate- $p_T$  region from  $0 < p_T < 6 \text{ GeV}/c$ , where a local maximum is observed, and the high- $p_T$  region for  $p_T > 6 \text{ GeV}/c$ , which is characterized by a strong rise and a subsequent saturation region. The following sections discuss these two momentum regimes separately.

## 2.1 High $p_T$ : Fragmentation, Jets and In-Medium Energy Loss

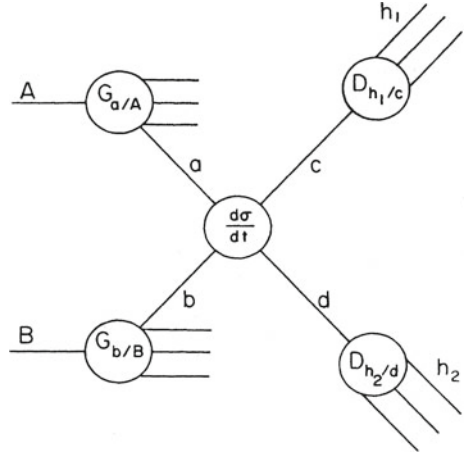
The high transverse momentum region of particle spectra is of special interest, since partons with high  $p_T$  are predominantly produced in scattering processes with high momentum transfer at the initial stage of the collision ( $Q \gg \Lambda_{\text{QCD}}$ ). In case of a pp collision, the underlying processes is possible to be calculated via pQCD, because a pp collision can be rather regarded as a collision of the partons in the vacuum. In case of heavy-ion collisions though, the hard scattering processes are embedded in the partonic medium, which builds up at the same time as the scattering takes place. The following interactions with the medium complicate the prediction of final hadron  $p_T$  spectra as compared to pp.

Nevertheless, the calculations of hard processes in pp serve as basic input for heavy-ion collision models. Therefore, the following paragraph is dedicated to the pQCD approach of calculating identified hadron high- $p_T$  spectra in pp collisions.

### Hard Scatterings in Elementary Reactions

On the basis of Feynman's parton model of hadrons [10, 11], in which the hadron consists of three point-like constituents, the partons, Bjorken has first described the hard scattering cross section of two hadrons (e.g. pp) for the inclusive reaction  $A + B \rightarrow h + X$  [12]: "Choose a collinear frame of reference in which the initial projectiles move relativistically and in opposite directions. Replace each projectile A, B by a beam of massless, non-interacting partons (a, b)... Regard the collision as a 2-body collision of a parton from each beam, the cross section depending only on [the momenta] of the interacting parton pair and independent of the rest of the environment of 'spectator' partons". In fact, the hadron reaction  $A + B \rightarrow h + X$  is regarded as if it was an inelastic parton scattering process  $a + b \rightarrow c + d$ . The successive formulation in [13] is completed with the convolution of the fragmentation function (FF), that describes the probability of the creation of a hadron  $h$  from a parton ( $c$  in this case) carrying away a fraction  $z$  of the parton momentum. The creation process is referred to as fragmentation, where the coloured parton fragments into colour neutral objects. In detail, the fragmentation of a parton implies the creation of  $q\bar{q}$  pairs via  $g \rightarrow q\bar{q}$ , gluon radiation ( $q \rightarrow qg$ ) or splitting ( $g \rightarrow gg$ ). The coloured remnants with distinctly lower momentum than that of the initial parton finally form colour neutral hadrons. The invariant cross section of identified hadrons as expressed in [13] is given here:

**Fig. 2.3** Schematic representation of a high  $p_T$  reaction factorized into parton distribution functions (G), parton fragmentation functions (D), and a hard scattering process. Figure and caption taken from [13]



$$E_h \frac{d^3\sigma}{dp_h^3}(A + B \rightarrow h + X) = \sum_{abcd} \int dx_a dx_b dz_c G_{a/A}(x_a) G_{b/B}(x_b) \cdot D_{h/c}(z_c) \frac{\hat{s}}{z_c^2 \pi} \frac{d\sigma}{d\hat{t}}(ab \rightarrow cd) \delta(\hat{s} + \hat{t} + \hat{u}), \quad (2.3)$$

$$\text{with } \left. \frac{d\sigma}{d\hat{t}} \right|_{\hat{s}} = \frac{\pi \alpha_s(Q^2)}{\hat{s}^2} \sum^{ab} (\cos \theta^*) \quad (2.4)$$

as the fundamental sub-process cross section,  $x_a = p_a/p_A$  as the momentum fraction of parton a from hadron A,  $G_{a/A}(x_a)$  as the probability of finding parton a in hadron A (parton distribution function PDF),  $D_{h/c}(z_c)$  as the FF of parton c into hadron h with the momentum fraction  $z_c = p_h/p_c$ .  $\sigma$  denotes the inelastic cross section of the interaction of parton a and b resulting in partons c and d. Finally, the delta function describes the two-body scattering of massless partons. In more detail, it describes the two-body phase space under the assumption that the initial and final partons are collinear with the initial and final hadrons, i.e. no transverse ( $k_T$ ) smearing is included [13]. The variables  $\hat{s}, \hat{t}, \hat{u}$  represent the so-called Mandelstam variables.<sup>3</sup> A sketch of the scattering process is shown in Fig. 2.3.

Although the parton model is based on pQCD, it assumes scale invariance of the PDFs and the FFs, which means that they are independent of  $Q^2$ ; only the scattering cross section has a scale dependence. This assumption originates from the so-called Bjorken scaling, where the structure functions, which describe the internal structure of the proton by combinations of different PDFs, are independent of  $Q^2$  for large parton momentum fractions,

<sup>3</sup>They are a different Lorentz-invariant formulation of the four momenta of the scattering particles with  $\hat{s} + \hat{t} + \hat{u} = 0$  for massless particles.

$$x = \frac{Q^2}{2M\nu} = \frac{Q^2}{2\mathbf{P}\mathbf{q}} \quad [14], \quad (2.5)$$

with  $M$  as the mass of the proton,  $\mathbf{P}$  as the proton four-momentum and the momentum transfer  $Q^2 = -\mathbf{q}^2$  or  $\nu$  as the energy loss of the scattering lepton, which is collided with the proton in order to reveal the internal structure of the proton. “This property is related to the assumption that the transverse momentum of the partons in the infinite-momentum frame of the proton is small. In QCD, however, the radiation of hard gluons from the quarks violates this assumption, leading to logarithmic scaling violations, which are particularly large at small  $x$ . The radiation of gluons produces the evolution of the structure functions” [14]. In order to introduce a scale dependence, which would allow the description of the cross section in a perturbative way, a so-called factorization procedure is applied. Consequently, the scale dependent FFs and PDFs can be related to measurements of identified hadron spectra, e.g. in  $e^+e^-$  collisions, and of the hadron structure functions from Deep Inelastic Scattering (DIS) of leptons with protons at a given  $Q^2$ . In case of the structure functions this yields:

$$F_2(x) \rightarrow F_2(x, Q^2) = \frac{1}{2} x \sum_q e_a^2 f_q(x, Q^2), \quad (2.6)$$

$$\text{where } f_q(x, Q^2) = q(x, Q^2) + \bar{q}(x, Q^2) \quad (2.7)$$

are the PDFs and  $e_a^2$  the electric charge of the quark with flavour  $q$  [14].

With regard to Fig. 2.3, on the one hand, the given process can be separated into a hard scattering that takes place between the interacting partons and that can be calculated perturbatively. On the other hand, in the assumed collinear configuration, the interacting quarks have a small relative momentum, which translates into a very strong interaction between them. Hence, pQCD is not applicable until a factorisation scale dependence is introduced, which separates for example the structure function into a part, that is calculable, depending only on  $Q^2$ , and into another part, which is not calculable but can be constrained by measurements. “The [factorisation] scale  $[\mu_F]$  can be thought as one which separates the perturbative short-distance physics from the non-perturbative long-distance physics. Thus partons emitted at small transverse momenta  $< \mu_F$  (i.e. approximately collinear processes) should be considered as part of the hadron structure. Partons emitted at large transverse momenta contribute to the short-distance part of the cross section which can be calculated” [15].

The structure functions measured by experiments, however, must be independent of the choice of  $\mu_F$ . Requiring the derivative of the structure function with respect to the scale  $\mu_F$  to be zero, the so-called DGLAP equation is obtained: Dokshitzer, Gribov and Lipatov, Altarelli and Parisi showed, that the structure function itself is not calculable but its changes with the factorisation scale are [16–19]. Despite the fact that the PDFs cannot be fully calculated via pQCD, the latter can predict how the distribution evolves as the scale varies via the DGLAP evolution. The DGLAP

evolution hence allows that the structure function at the scale  $Q$  can be expressed by the structure functions measured for example in DIS at a given scale  $Q_0$ , which can be lower than  $Q$ . Usually the factorization scale is chosen to be  $\mu_F = Q$ .

The cross section from Eq. 2.4 for partons  $a + b \rightarrow c + d$  can be calculated in a perturbative manner from the incoherent summation over all possible constituent scatterings above the given momentum transfer limit. Similarly to the PDFs, the FFs are obtained from fits of theoretical calculations to identified hadron spectra from  $e^+e^-$  collisions in this case. However, the calculation of the FFs is accompanied by additional difficulties as compared to the PDFs, because the hadronisation process is sensitive to physics happening at long distances, where pQCD starts not to be applicable any more. Moreover, the kinematic reach of data by which the FF can be constrained, is more limited as it is the case for the PDFs [20]. On the other hand, the FF for the vacuum are expected to be universal and hence independent of the collision system [14].

Hadrons produced from hard-scattered partons follow a power-law function,

$$E_h \frac{d^3\sigma}{dp_h^3} \propto p_T^{-n} F(x_T), \quad (2.8)$$

where  $x_T = 2p_T/\sqrt{s}$ . A power-law behaviour was first proposed by BBK [21] and is still confirmed by recent measurements [22]. The power-law shape of the hadrons is a result of the power-law shaped distributions of the scattered partons, where the power  $n$  from the parton spectrum is maintained [20].

The NLO calculations for jet and particle spectra in pp are well advanced. Recent calculations are able to describe jet spectra for a wide range of energies, ranging from  $\sqrt{s} = 0.2 - 7$  TeV, with reasonable accuracy and moderate systematic uncertainties [14, 22]. In case of pp  $p_T$  spectra though, NLO does not agree well with the data, but is able to reproduce the relative dependence on  $p_T$  of cross sections of two collision energies [22]. A profound understanding of processes and their description with pQCD, respectively, is however an important ingredient for the investigation of AA collisions.

### Nuclear Parton Distribution Function

For the calculation of AA collisions, instead of the PDFs, the nuclear parton distribution functions (nPDF) are needed as input. They are related to the hadron PDFs via a scaling factor, that is also depending on  $x$  and  $Q^2$ :

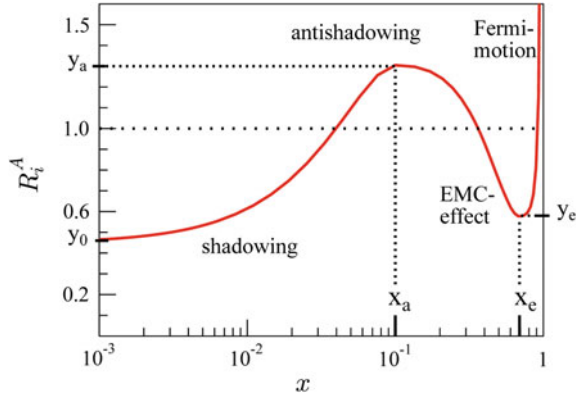
$$f_i^A(x, Q^2) \equiv R_i^A(x, Q^2) f_i(x, Q^2) \quad (2.9)$$

with  $i$  the quark flavour and  $A$  the mass number of the nucleus. Figure 2.4 shows a sketch of the evolution of  $R_i^A(x)$  with  $x$ . At values of  $x \ll 0.1$  a depletion or “shadowing” is observed, which evolves to a “anti-shadowing” around  $x \approx 0.1$ . This is followed by the “EMC-effect<sup>4</sup>” in the range of  $0.2 < x < 0.7$  causing a

---

<sup>4</sup>European Muon Collaboration.

**Fig. 2.4** A sketch of the EPS09 fit functions  $R_i^A(x)$  (with  $i$  as the parton flavour) and the role of certain fit parameters. Figure and caption taken from [23]



depletion. The final rise is generated by the “Fermi motion” leading to an excess at  $x = 1$ . The shadowing at low  $x$  is also referred to as one of the cold nuclear matter effects, that modify the initial parton distributions as compared to pp. This modification is distinguished from the modification due to the presence of a hot medium. The invariant cross section in p–A collisions, which could be regarded as a “cold” collision, would scale linearly with the cross section in pp  $\sigma_{pA} = \sigma_{pp} A$  if no nuclear matter effects were expected. As far as Fig. 2.4 is concerned, this is clearly not the case; in fact, the relation is rather given by  $\sigma_{pA} \propto \sigma_{pp}^A$ . Another definition of  $x = p_T/\sqrt{s} \cdot e^{-y}$  ( $y$  is the rapidity) shows, that at the LHC lower values of  $x$  are probed as at RHIC or at the SPS if the same  $p_T$  is regarded and thus different nuclear matter effects become important.

Recent calculations of the  $R_i^A(x, Q^2)$  parameter are delivered by the EPS09 collaboration [24], who work with results from DIS and measurements from d–Au collisions at RHIC. The calculations are based on a NLO global DGLAP analysis of nPDFs. “In the lack of sufficient data constraints, we are forced to start with only three different modification ratios:  $R_G^A(x, Q^2)$ ,  $R_V^A(x, Q^2)$ , and  $R_S^A(x, Q^2)$  for gluons, valence quarks and sea quarks, correspondingly. The  $A$  dependence is embedded in the  $A$  dependence of the parameters” [23]. Despite the fact that the recent results of the nPDFs are in good agreement with measurements, the nPDFs are not yet available for all centralities, which is essential for describing the QGP evolution and properties.

Concerning the FF from nuclei (nFF), no significant theoretical output is available yet. Instead of nFF, the FF from the vacuum are used and folded with a medium influence in order to describe AA collisions. Vital for the determination of nPDFs and nFFs is the distinction of effects that originate from processes in the vacuum and from the influence of cold or hot nuclear matter, which can only be sorted out by future measurements.



## Hard Scatterings and Energy Loss in Heavy-Ion Collisions

Resuming the discussion above, the basic ingredients for the calculation of the particle production in Pb–Pb collision seem to be available, if no effects introduced by the hot medium, e.g. the QGP, are expected. That the latter is not the case was already explained in the context of the above-mentioned energy-loss scenarios.

High- $p_T$  partons are predominantly created in hard scatterings at the initial stage of the collision. The recipe for the invariant cross section of particle production at high  $p_T$  in Pb–Pb collisions thus contains a hard scattering pQCD process as discussed in the previous section and the influence of the QCD medium in which the process is embedded. A simplified description of the invariant cross section for the creation of a hadron  $h$  under the assumption that the initial parton fragmentation is modified by the medium via the energy loss  $P(\Delta E(Q^2, E))$  approximation,

$$\text{FF}_{h/c}^{\text{med}}(z_c, Q^2, E_c) \approx \int_0^E d(\Delta E) P(\Delta E(Q^2, E_c)) \text{FF}_{h/c}^{\text{vac}}(z_c - \frac{\Delta E}{E_c}, Q^2), \quad (2.10)$$

is presented here:

$$E_h \frac{d^3\sigma}{dp_h^3}(A + B \rightarrow h + X) \approx \sum_{abcd} \int dx_a dx_b dx_c \text{nPDF}_a(x_a, Q^2) \text{nPDF}_b(x_b, Q^2) \cdot \text{FF}_{h/c}^{\text{med}}(z_c, Q^2, E_c) \sigma(Q^2)(ab \rightarrow cd). \quad (2.11)$$

Within this approximation, the fragmentation process is not modified, but the parton momentum is changed by the energy loss. The FF obtained from fits to measured results from elementary collisions, i.e.  $e^+e^-$ , as for example by AKK [25], are used instead of the nFF due to large uncertainties of the latter as explained earlier. The parameter, which shows the largest uncertainty, is the medium-induced energy loss  $P(\Delta E(Q^2, E))$ . Understanding and quantifying this medium property as well as the applicability of pQCD for the given process are among the major challenges in the field.

In order to quantify the medium-induced energy loss, two effects are commonly considered [26]:

- incoherent collisional energy loss ( $\sim$ elastic scattering)
- coherent radiative energy loss ( $\sim$ inelastic scattering),

which are sketched in Fig. 2.5. Whereas the collisional energy loss from elastic scatterings with thermal partons, i.e. partons not stemming from hard scatterings, affects mainly partons at lower momenta [5], the radiative energy loss is commonly thought to be dominant for high- $p_T$  partons with  $p_T > 5$  GeV/c. Gluons and light quarks, such as u, d, s, are expected to lose energy rather via bremsstrahlung (quarks) or medium-induced gluon radiation (both), respectively, than from elastic scatterings. This is opposite to heavy quarks (c, b), where the radiative loss is supposed to be

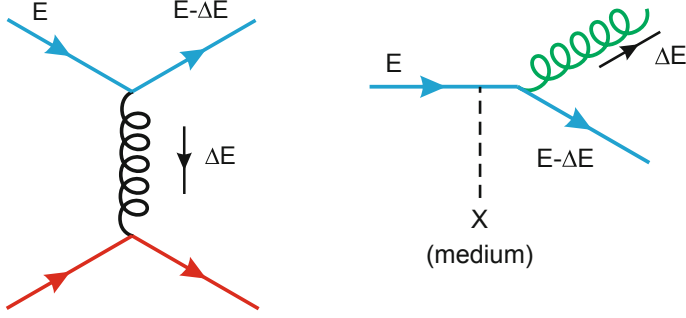


**Fig. 2.5** Diagrams for collisional (*left*) and radiative (*right*) energy losses of a quark of energy  $E$  traversing a quark-gluon medium. Figures and caption from [26]

reduced by the so-called dead-cone effect [27] and thus collisional effects could dominate, which are mass dependent [28].

The inelastic radiation process induced by multiple scatterings involves gluons, that are coherently radiated in a bremsstrahlung-like interaction. This is expressed in pQCD for a large medium as compared to the mean free path  $\lambda$  ( $L \gg \lambda$ ) via the Landau–Pomeranchuk–Migdal (LPM) formalism [29, 30]. The LPM effect is expected to cause a quadratic path or formation length ( $L$ ) dependence of the mean radiative energy loss [26]:

$$\langle \Delta E_{\text{med}}^{\text{LPM}} \rangle \approx \alpha_s \hat{q} L^2 \quad (\sim L^2 T^3 \quad [70]), \quad (2.12)$$

with the transport coefficient, governing the transverse momentum diffusion of a fast parton per unit path length,

$$\hat{q} = \frac{\langle q_{\perp} \rangle^2}{\lambda}, \quad (2.13)$$

where  $\lambda$  is the mean free path given by  $1/(\sigma\rho)$ , with  $\rho$  as the density, and  $\langle q_{\perp} \rangle$  as the mean transverse momentum transferred from the medium to the parton per collision.  $\langle q_{\perp} \rangle$  characterizes the typical momentum exchange with the plasma. However, it has not been clarified yet, if the total radiative energy loss really depends on  $L^2$  or on another power of the path length. The additional power of  $L$  as compared to the collisional energy loss is one of the main reasons why the radiative energy loss is considered to dominate [31]. According to [32],  $\hat{q}$  could be thought to be energy-dependent, although it appeared to describe the measurement only for very high  $p_T$ .

Consequently, the gluon radiation needs to be tracked through the medium in order to reveal the medium density and transport properties, that are both linked to  $L$ . For the experimental realization, observables of the radiative energy loss are vital

and have to be defined. This leads to the definition of “jets”, which will be explained in the following section.

Summarizing this paragraph, for the understanding of the medium properties, the following aspects of partonic energy loss need to be understood: path length dependence, space time evolution and geometry, which influence the path length, quark-gluon difference, difference of vacuum and in-medium radiation and the contributions of the collisional and radiative energy loss to the total energy loss.

### Jets and Radiative Energy Loss

A jet originates from a hard scattering parton, which produces a collimated parton shower via the fragmentation process finally creating colour neutral particles with subsequently lower momenta than the original parton momentum. The jet is defined by a certain angular region, recovering the parton energy by the summation over all produced particles in this region. The jet cone is determined by the distance parameter  $R$ . The collimation into a jet-like shape is caused by the strong scale dependence of the coupling, which leads to a suppression of large-angle radiation. In reality, however, the full reconstruction of the parton energy is only possible in pp collisions, because in heavy-ion collisions, the radiative energy loss of the parton in the medium plays a major role.

The effect of radiative energy loss on a hard scattered parton can be visualised by the measurement of the jet  $R_{AA}$ . Basically, there are two scenarios:

- $R_{AA} = 1$  as a result of jet broadening in transverse direction caused by in-cone radiation in the medium. From these radiated gluons fragmenting outside the medium (as the leading parton), the initial leading parton spectrum can still be recovered.
- $R_{AA} < 1$  due to out-of-cone radiation, which results into a modified jet  $p_T$  spectrum and finally to a suppression of the yield in a given  $p_T$  range as compared to pp.

As Fig. 2.2 shows, the jet  $R_{AA}$  at the LHC is compatible with that of inclusive charged particles. In detail, the jet suppression is also around 0.5, hinting to out-of-cone radiation. This could also include the absorption of the radiated gluons by the medium. The saturation of the jet and hadron spectra  $R_{AA}$  at very high  $p_T$  is not yet fully understood and currently under investigation [32].

Apart from the nuclear modification factor as a function of  $p_T$ , there is the so-called  $I_{AA}$  parameter used for di-jet studies. Also here, a strong suppression is observed: Di-jets are two jets which are assumed to originate from the same scattering process wherein they were produced with opposite transverse momenta. Hence, their constituents are correlated not only within one jet but also between the two jets. A correlation analysis (di-hadron analysis) is usually performed by selecting a trigger particle with a given (high) momentum and calculating the angular difference in azimuthal direction between this particle and all others of lower momenta,  $\Delta\phi = \phi_{\text{trig}} - \phi_{\text{assoc}}$ . From this angular difference, two regions in  $\Delta\phi$  can be distinguished: the near-side peak around zero and the away-side peak around  $\pi$ . If the integrated yield at the near or away side in AA collisions is divided by that in pp collisions, the parameter  $I_{AA}$  is obtained, in analogy to  $R_{AA}$  for the  $p_T$  spectra.  $I_{AA}$  is commonly studied as function of the trigger particle's  $p_T$  or of centrality. In pp collisions, the amplitude

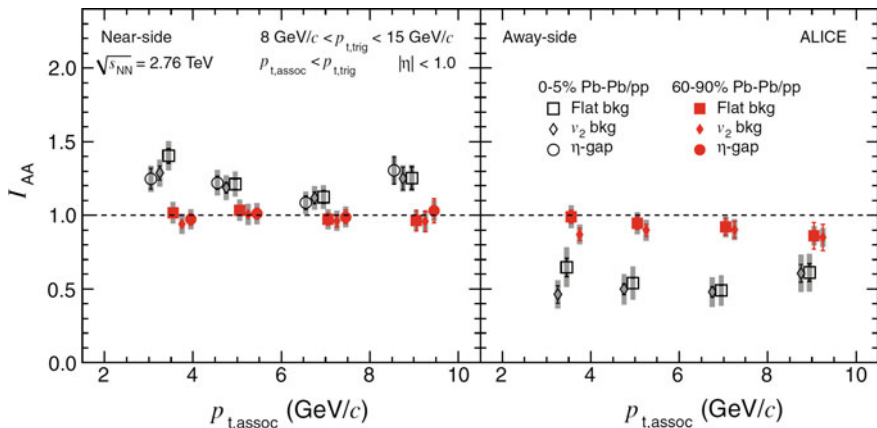


**Fig. 2.6**  $I_{AA}$  for central (0–5% Pb–Pb/pp, *open black symbols*) and peripheral (60–90% Pb–Pb/pp, *filled red symbols*) collisions. Results using different background subtraction schemes are presented: using a flat pedestal (*squares*), using  $v_2$  subtraction (*diamonds*) and subtracting the large  $|\Delta\eta|$ -region (*circles*, only on the near-side). For clarity, the data points are slightly displaced on the  $p_{T,assoc}$ -axis. The *shaded bands* denote systematic uncertainties. Figure and caption taken from [33] (color figure online)

of both peaks is of the same order, whereas in Au–Au collisions, the away-side peak is suppressed by a factor of 3–5 at RHIC [34, 35]. The unmodified near-side peak is a result of the trigger particle procedure, where with the trigger particle selection, partons from or close to the surface are selected, which did not encounter energy loss. Their path length is hence much smaller than that of the recoiled parton, which had to travel basically through the whole medium and suffered strong energy loss. Therefore, one could think of the sensitivity of this measurement to the path length dependence of the energy loss. Though, during the long travel through the medium, the medium properties, i.e. its density, could have already changed due to the rapid expansion. Interestingly, the shape of the away side peak equals that in pp for trigger particles with  $p_T \gtrsim 7 \text{ GeV}/c$ .

In case of LHC, a suppression of 0.6 for the away side and a slight enhancement of 1.2 for the near side in central collisions has been reported by ALICE as seen in Fig. 2.6. The latter feature is observed for the first time [33] and could hint to a higher  $Q^2$  in the medium than in vacuum. For peripheral collisions, no suppression for the near-side peak and only a small suppression ( $\sim 0.9$ ) is found for the away-side peak indicating that this system is either smaller or less dense than in central collisions. Remarkable is, that the  $I_{AA}$  is much smaller in central collisions at RHIC than at the LHC, while this is not the case for  $R_{AA}$ . The lower away-side  $I_{AA}$  suggests that the medium is more opaque or stronger coupled at RHIC [36]. Since the  $R_{AA}$  represents a less differential observable, which integrates over the near- and away-side, the rather similar  $R_{AA}$  at both energies hints to a larger contribution from partons closer

to the surface (for which the loss of energy is generally less) to the  $R_{AA}$  than to the away-side  $I_{AA}$ .

### Attempts of Basic $R_{AA}$ Interpretation

For a basic understanding of the influence of the energy loss on the spectra and thus on  $R_{AA}$ , two simplified energy loss scenarios are considered in the following.<sup>5</sup> The nuclear modification factors are calculated assuming a power-law behaviour of the parton and consequently also of the hadron spectrum with  $E d^3\sigma/d^3p_T \propto p_T^{-n}$ , which corresponds to  $dN/dp_T \propto p_T^{-(n-1)}$ :

#### 1. Constant energy loss

$$\begin{aligned} p'_T &= p_T + \Delta E/c \\ \Rightarrow R_{AA} &= C + \left( \frac{1}{1 + \Delta E/p_T c} \right)^{(n-1)}. \end{aligned} \quad (2.14)$$

After the energy loss, the yield at a given  $p_T$  in AA corresponds to the yield in pp at a higher  $p'_T$ , which is lower than that at  $p_T$  in pp. The constant  $C$  accounts for the relative amount of partons very close to the surface, that could escape without being affected by the medium [9].

#### 2. Constant fractional energy loss [38]

$$\begin{aligned} p'_T &= p_T + S(p_T) \quad \text{with} \quad dS/dp_T = S_0 \\ \Rightarrow R_{AA} &= C + \left( \frac{1}{1 + S_0} \right)^{(n-2)} \end{aligned} \quad (2.15)$$

The constant fractional energy loss  $S_0$  can be substituted by an effective fractional energy loss  $S_{loss}$  via the relation  $S_{loss} = S_0/(1 + S_0)$ , leading to

$$R_{AA} = C + (1 - S_{loss})^{(n-2)} \quad (2.16)$$

$$\Rightarrow S_{loss} = 1 - (R_{AA} - C)^{\frac{1}{n-2}}. \quad (2.17)$$

In the first case, the constant energy loss leads to a  $p_T$ -dependent suppression. Since  $\Delta E/p_T$  decreases with larger  $p_T$ ,  $R_{AA}$  is expected to increase and to finally approach unity [1] depending on  $n$ . In the second case of constant fractional energy loss, the measured spectrum shifts towards lower  $p_T$ . For a pure power-law spectrum this yields a constant  $R_{AA}$ , which is indeed observed at  $p_T > 30 \text{ GeV}/c$  (see Fig. 2.2). For a growing fractional energy loss with  $p_T$ , the slope of  $R_{AA}$  is softer than for the case of constant energy loss. Consequently, the slope of  $R_{AA}$  contains valuable information about the momentum (energy) dependence of the energy loss. The sensitivity to the details of parton energy loss is strongly correlated with the power  $n$  of

---

<sup>5</sup>This discussion is inspired by Macro van Leeuwen's lectures within the Helmholtz Research School for Quark Matter Studies in Heavy Ion Collisions (HQM) lecture week series [37].

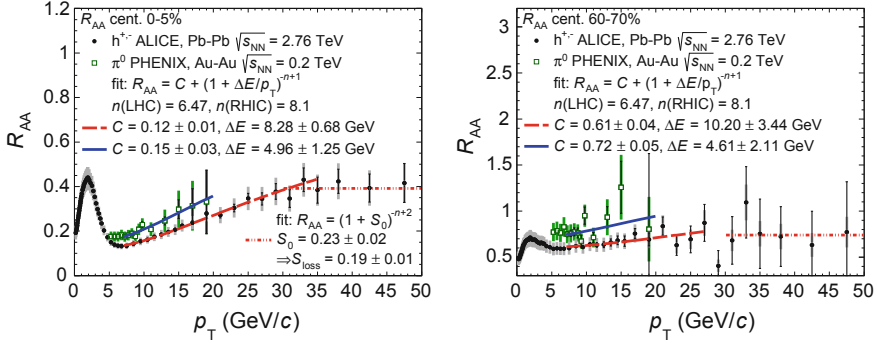


**Fig. 2.7** Nuclear modification factor of charged particles measured by ALICE [7] and of neutral pions measured by PHENIX [40] fitted with Eq. 2.14 for the case of constant energy loss (*full*, *dashed line*) and with Eq. 2.15 (*dashed-dotted line*)

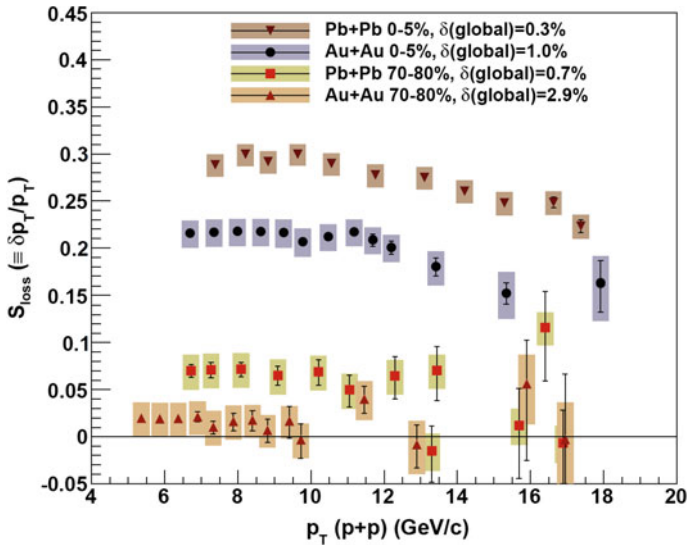
the parton spectrum, therefore the extraction of the energy loss from measurements is not straightforward. It has to be clarified if the observed  $R_{AA}$  is a result from a combination of both discussed scenarios and if the assumption of a pure power-law with the same  $n$  for all  $p_T$  is correct [32]. In case of ALICE jet measurements, a slightly smaller exponent is observed for  $p_T = 20 - 125$  GeV/c than for the charged particle spectra with  $p_T < 30$  GeV/c [22, 39].

Figure 2.7 shows the  $R_{AA}$  of charged particles measured by ALICE [7] together with the neutral pion<sup>6</sup>  $R_{AA}$  in Au-Au collisions at  $\sqrt{s_{NN}} = 200$  GeV published by PHENIX [40]. Both  $R_{AA}$  are fitted with the function of Eq. 2.14 in order to extract the constant energy loss  $\Delta E$  and the fraction  $C$  of partons with unmodified  $p_T$ . At RHIC,  $n = 8.1$  [38], while at the LHC  $n = 6.47$  is measured [22] for  $p_T < 30$  GeV/c. The results for  $C \approx 0.12$  seem to be similar for RHIC and LHC energies for both centralities within the uncertainties. However, the value of  $C$  in central collisions increases for peripheral collisions by a factor 4–5. Since a smaller, less dense medium (if at all) is expected for peripheral collisions, more partons could fragment outside the medium and/or stem from parts, where they suffered no energy loss. The energy loss at RHIC and the LHC remains rather constant for both centralities, whereas at the LHC  $\Delta E$  is almost twice as large as at RHIC, where  $\Delta E \approx 5$  GeV. If  $C$  is neglected in the fit, the energy loss reduces from 5 to 2.3 GeV at RHIC and from 8.3 to 5 GeV at the LHC. Due to the large uncertainties of RHIC measurements, it is not yet possible to conclude, if the  $R_{AA}$  becomes similar to the LHC  $R_{AA}$  above 12 GeV/c, which would influence the slope of the fit and hence the extracted energy loss. In case of the ALICE measurement in Fig. 2.7, the plateau above  $p_T = 30$  GeV/c was additionally fitted with Eq. 2.15. For central collisions  $S_{\text{loss}} = 0.2$  and for peripheral  $S_{\text{loss}} = 0.07$  was extracted with  $C = 0$ . Thus, if all partons lost energy in the medium, the mean fractional energy loss would be 20 % (7 %) as compared to the original  $p_T$  in pp col-

<sup>6</sup>A neutral pion,  $\pi^0$ , consists of a mixture of  $d\bar{d} + u\bar{u}$  quarks. Its  $R_{AA}$  is hence comparable to the charged particle  $R_{AA}$ .

lisions. If 88 % (39 %) of the partons were affected in central (peripheral) collisions, the fractional loss would be 25 % (40 %) instead. These simple considerations show the need for further investigations concerning the disentanglement of the different modification options and the contribution of unmodified partons to the observables.

The energy loss can also be considered to be a  $p_T$ -dependent momentum loss. This is expressed by the  $p_T$ -dependent momentum difference in AA and pp collisions  $\delta p_T = p_T(\text{pp}) - p_T(\text{AA})$  as suggested in [40]. In Fig. 2.8, the comparison of  $S_{\text{loss}} = \delta p_T / p_T(\text{pp})$  in central and peripheral collisions measured by PHENIX for  $\pi^0$  at  $\sqrt{s_{\text{NN}}} = 0.2 \text{ TeV}$  and by ALICE for charged particles at  $\sqrt{s_{\text{NN}}} = 2.76 \text{ TeV}$  is shown as a function of the  $p_T$  in pp collisions.  $S_{\text{loss}}$  was extracted by employing a fit with a power-law function to the  $\langle T_{\text{AA}} \rangle$  scaled spectrum in pp collisions and by calculating the horizontal shift to the spectrum in Au–Au at each  $p_T$  in pp collisions. The relative momentum change is constant below 12 GeV/c for all centralities and collision energies. Only in central events a slight decrease is observed above this  $p_T$ , which is consistent with the slow rise of  $R_{\text{AA}}$ . Although the  $R_{\text{AA}}$  is similar above 10 GeV/c for LHC and RHIC energies,  $S_{\text{loss}}$  is 30 % lower at RHIC, which could be a result of the different  $n$  of the power-laws. Assuming that the fragmentation of the initial parton remains unchanged after the energy loss, the fractional momentum loss can be interpreted as average fractional energy loss of the initial parton [40].



**Fig. 2.8**  $S_{\text{loss}} = \delta p_T / p_T$  for charged particles from ALICE [41] and for  $\pi^0$  measured by PHENIX [40]. The error bars are statistical, the boxes around the points indicate systematic uncertainties. Figure taken from [40]. The coloured lines at high  $p_T$  mark the results from fits with Eq. 2.15 with  $C = 0$  to the ALICE  $R_{\text{AA}}$  in central (green) and peripheral (blue) collisions

In [42], an estimation procedure for the lower limit of  $R_{AA}$  is introduced, which can be regarded as a geometrical limit of  $R_{AA}$ . This universal bound model considers hadrons above  $p_T = 5 \text{ GeV}/c$ , where the collective flow effects (see Sect. 2.2) are no longer expected to contribute. The lower bound of  $R_{AA}$  is given by

$$R_{AA}^{\text{geom}} = k \frac{N_{\text{part}}}{2 N_{\text{coll}}} \propto N_{\text{part}}^{-1/3}, \quad (2.18)$$

where the constant factor  $k$  “is an adjustable parameter of order unity; its numerical value is universal for all particles (except perhaps for hadrons containing b quarks at moderate  $p_T$ ) and is determined by the thickness of low-density ‘corona’” [42]. In order to obtain  $R_{pp} = k$ , the factor 2 in the denominator is inserted. Since  $R_{pp}$  is expected to be 1,  $k$  should also be of the order of 1.

$R_{AA}^{\text{geom}}$  is based on the following dependences given by the Glauber model, which is referred to again in Sect. 3.5: The volume  $R^3$  is proportional to  $N_{\text{part}}$  and thus the surface to volume ratio is  $\propto N_{\text{part}}^{-1/3}$ . Taking into account that  $N_{\text{coll}} \propto N_{\text{part}}^{4/3}$ , one obtains  $N_{\text{part}}^{-1/3} = N_{\text{part}}/N_{\text{coll}}$ . The model describes the lower bound of the data at high  $p_T$  quite well with  $k = 1.0$ , as shown in Fig. 2.9. A question arising from this is, if this is also true for other particle species than those containing u and d quarks and if this limit is universal.

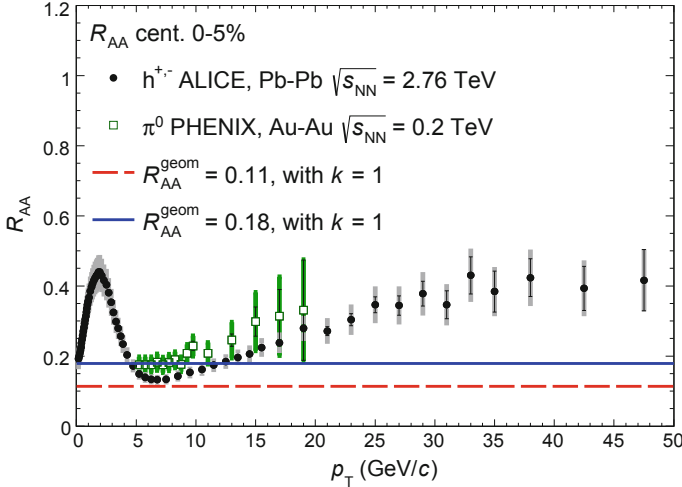


**Fig. 2.9** Nuclear modification factor of charged particles from ALICE [7] and of  $\pi^0$  measured by PHENIX [40]. The error bars are statistical, the boxes around the points indicate systematic uncertainties. The lines marks the geometrical limit as calculated in [42] with  $k = 1$



The findings with regard to the nuclear modification factor at high  $p_T$  from RHIC and the LHC are summarized in the following:

- **RHIC:**  $R_{AA}$  seems to slightly rise with  $p_T$ , following the lower bound (see Fig. 2.9) given by the geometric limit from 5 to 12 GeV/c, which hints to surface emission, i.e. only particles stemming from partons produced close to the surface of the medium contribute to the particle yield at these  $p_T$ . The remaining partons are absorbed such, that their energy is shifted to lower momenta contributing to the thermal background. The approximate flatness of  $R_{AA}$  with  $p_T$  could also be the result from a spectrum shift by fractional energy loss. However, within the present uncertainties, this remains a guess. At  $p_T > 12$  GeV/c, the suppression is similar to that at the LHC within the uncertainties. Nonetheless, the modification in central events for both energies is strong ( $R_{AA} \approx 0.2 - 0.4$ ), indicating that the medium is almost opaque and absorbs a lot of the energy of a fast trespassing parton. The fit to the  $R_{AA}$  assuming a constant parton energy loss yields  $\Delta E \approx 5$  GeV/c (2.3 GeV/c) for  $C = 0.15$  (0), the fraction of partons fragmented outside the medium or unaffected by energy loss, which corresponds to the estimate of the lower bound of  $R_{AA}$  within the systematics.
- **LHC:**  $R_{AA}$  of unidentified charged particles is significantly  $p_T$ -dependent, the geometrical limit is only touched at  $p_T = 6 - 7$  GeV/c (see Fig. 2.1). The deviation from the constant geometrical limit at lower  $p_T$  could be a result of the steeper slope parameter of the assumed power-law shaped spectrum. A constant behaviour is observed for  $p_T \gtrsim 30$  GeV/c at a suppression of  $R_{AA} \approx 0.4 - 0.5$  [43], as seen in Fig. 2.2. According to [1], “at hypothetically large  $p_T$  when the total energy loss is negligible compared to the initial jet energy, the ratio should approach to one”. This still needs to be clarified by measurements at  $p_T > 300$  GeV/c, which is expected to be the case during the data recording period starting in 2015. The fit to the  $R_{AA}$  assuming a constant parton energy loss yields  $\Delta E \approx 8$  GeV/c, which is almost twice as much as at RHIC indicating a more opaque medium at the LHC. Also at the LHC, the estimate of the lower bound of  $R_{AA}$  corresponds to the fraction  $C = 0.12$ .

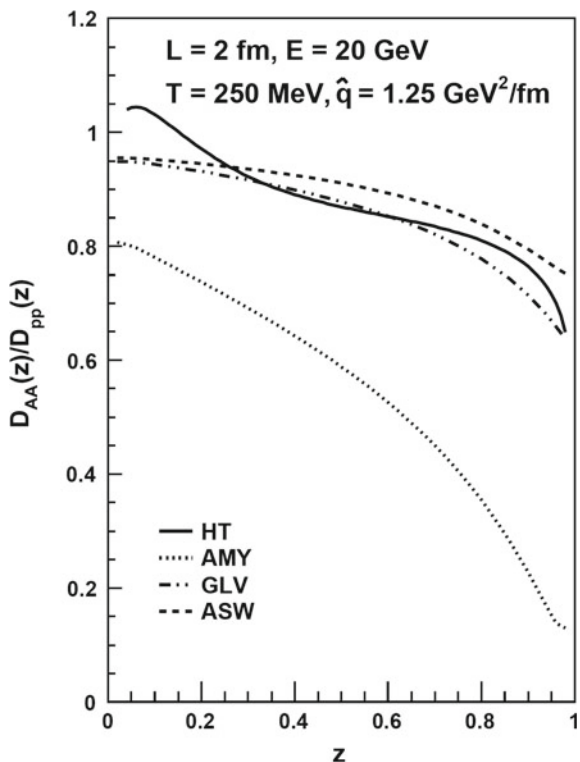
Summarizing the models for parton energy loss contained in Fig. 2.1, such as models based on a leading-parton energy loss description for elastic energy loss ( $\propto L$ , e.g. [44]), radiative energy loss ( $\propto T^3 L^2$ , e.g. (D)GLV [45, 46], ASW [47], AMY [48], HT [49–51], YaJEM [52]), both mechanisms (WHDG [30]) and strong coupling ( $\propto T^4 L^3$  in AdS/CFT<sup>7</sup> [53]), the resulting  $p_T$  dependence of  $R_{AA}$  in these models from intermediate to high  $p_T$  is comparable. Concerning the charged particle  $R_{AA}$  at the LHC in Fig. 2.1, most of the mentioned models are able to reproduce the shape but not the overall magnitude of the modification. Whereas the values obtained by the elastic energy loss models are above the data at low  $p_T$ , the radiative and strong coupling models overestimate the suppression.

Taking into account the results from RHIC and the LHC at the same time, it seems that the favoured power of  $L$  is  $1 < n \leq 2$  [31], which would mean that the

<sup>7</sup>Anti de-Sitter conformal field theory (string theory).

radiative energy loss dominates over the other energy loss processes depending on higher orders of  $L$ . The dominance of elastic energy loss however is thought to be possible for heavy quarks [54]. A clear distinction between the parton distribution modified by the path length depended energy loss, a possibly modified fragmentation and the contribution from partons fragmenting in- and outside the medium is difficult [1]. Therefore it is questionable if the path length and temperature dependence can be extracted at all from  $R_{AA}$ . Concerning the radiative energy loss in the above-mentioned models, “in addition to the microscopic model of the medium, a realistic calculation of energy loss in heavy-ion collisions also requires a macroscopic model of the medium, specifying the space-time dependence of the local properties of the plasma” [55]. For the same parameters, the radiation formalisms yield different modified fragmentation functions as it can be seen in Fig. 2.10, which demonstrates the difficulty of modelling the plasma properties, as for example the medium response to a trespassing parton, and the need for constraints from reliable measurements. It should be kept in mind that the description of  $R_{AA}$  by models is not enough, a complete understanding is only possible if all observables can be described simultaneously. This includes  $R_{AA}$  and  $I_{AA}$  as well as the hadron  $p_T$  spectra, the flow (see next Sect. 2.2), the (relative) particle abundances and particle correlations.

**Fig. 2.10** Comparison of quark fragmentation function ratios using four different formalisms for a uniform medium with  $L = 2$  fm and  $T = 250$  MeV. Figure and caption taken from [55]



## Energy Loss and Flavour Dependence

Until now, no distinction with regard to the particle flavour was made. However, the investigation of flavour dependent energy loss and the dependence on the number of constituent quarks is important as well. Are the above-mentioned observations universal in this respect?

The colour coupling factor for gluons given by QCD is larger by  $9/4$  as compared to quarks. Thus, the QCD medium induced energy loss should consequently be smaller for quarks than for gluons resulting in a smaller suppression for quarks. Moreover, “the gluon density inside nucleons at small  $x$  is larger than for quarks; the gluon-gluon scattering cross section is larger than the quark-quark; and a gluon jet produces more [soft] particles than a quark jet” [1]. In addition, the fragmentation functions by AKK and KKP [56] show, that for baryons the contribution of gluon fragmentation is larger than for mesons.

The following research questions can be deduced from this discussion: Is the energy loss independent of the quark mass and thus of the quark flavour? Is the suppression different for hadrons predominantly stemming from quark fragmentation to those from gluon fragmentation, i.e. is there a difference in the modification for baryons and mesons? Is a flavour or parton type dependent energy loss possible to be translated into the suppression measured from identified hadrons?

Referring to the first question, in case of heavy quarks the energy loss is expected to be even smaller than for light quarks due to the dead-cone effect [27]. This is supposed to reduce small-angle gluon radiation for heavy quarks (already in the vacuum). The medium influence is consequently smaller and thus decreasing the suppression. A competing effect is the in-medium hadron formation and dissociation or melting [57], which takes place at later stages as the initial scattering processes but being faster than the light-flavour formation times. Which mechanism dominates is left to be clarified. Concerning the second and third question, the particle production mechanisms need to be considered: Either the constituent quarks of the hadron could have lost energy before forming the hadron (recombination picture, see Sect. 2.2) or the parton fragmenting into the hadron could have suffered energy loss. The translation of the observed identified hadron suppression to the energy loss is hence only possible, if the production mechanisms of the hadrons are definite. In case of fragmentation, the fraction of gluon and quark fragmentation leading to the hadron production as well as the momentum distribution of the partons contributing to the hadron formation need to be known. As explained earlier, this knowledge is available from the fragmentation functions as determined by various groups [25, 56]. Since the fragmentation process does not link a hadron  $p_T$  directly with the parton  $p_T$  it is created from—an integration over the parton  $p_T$  is needed (see Eq. 2.4)—the energy loss cannot be extracted from the  $R_{AA}$  if it is parton energy dependent. Consequently, the trial and error principle perhaps seems to be the best opportunity, which means in detail, that the energy loss needs to be modelled by theory and the resulting  $R_{AA}$  eventually to be compared to measurements.

First it has to be clarified if  $R_{AA}(h(u,d)) = R_{AA}(h(s))$  and whether this implies  $\Delta E(u, d) = \Delta E(s)$ . Additionally the question could be raised if the baryon and the

meson  $R_{AA}$  are equal at high  $p_T$ . In [58], for example, the proton  $R_{AA}$  was calculated to be smaller than the pion  $R_{AA}$  at RHIC, which was mainly caused by the different fragmentation functions. Moreover, at present it is not clear, whether the energy loss of light quarks is larger than that of heavy quarks and if this furthermore results into

$$R_{AA}(h(\text{light quarks})) < R_{AA}(h(c)) < R_{AA}(h(b)) \quad (2.19)$$

above  $p_T = 10 \text{ GeV}/c$ . One idea behind is that at high momenta ( $p_T \geq 10 \text{ GeV}/c$ ), the heavy-quark masses contribute more to the total hadron  $p_T$  than light quark masses at the same  $p_T$ . Thus, if the energy loss increases with the velocity as it could be the case for the collisional energy loss [28], the heavy-quark hadron suppression can be thought be smaller than that of light-quark hadrons. On the other hand, in addition, the above-mentioned dead-cone effect, reducing the contribution from radiative energy loss for heavy quarks plays a role for this ordering. However, recent calculations [59] weaken the importance of the dead-cone effect by showing that the radiative gluon emission does play a significant role for heavy quarks from intermediate to high  $p_T$ . Moreover, it is stated that the dead-cone effect is only predominantly present at lower  $p_T$  though being much “less important than originally advocated”. On these grounds, the measurement and comparison of the mentioned differently flavoured particles  $R_{AA}$  is expected to provide a test of the colour-charge and mass dependence of parton energy loss and may help to constrain model calculations on fragmentation mechanisms in the system evolution of hot and dense nuclear matter. This implies the path length dependence inside the created medium, the flavour and colour charge dependence of the energy loss of the interacting partons surrounded by the medium. From this, with the help of models it could be possible to constrain the medium density and transport parameters. And finally it has to be clarified if also the fragmentation is modified by the medium besides the parton spectrum or if the fragmentation happens exclusively outside the medium. Important for that is the understanding of the dynamical evolution of the system and the complete picture of the partonic final-state interactions.

## 2.2 Low $p_T$ : Initial State Effects and Bulk

In the lower momentum region, the application of pQCD as well as the description of the hadronisation process via the fragmentation functions is no longer valid. The so-called bulk medium consisting of partons with mean  $p_T$  or a temperature, respectively, of around  $200 \text{ MeV}/c$  (at RHIC and LHC energies) is created at the early stage of heavy-ion collisions, right after the initial hard scatterings. The bulk is considered to be strongly gluon dominated as a result of the nPDFs. The measured hadron spectra at low  $p_T$  ( $p_T \lesssim 2 \text{ GeV}/c$ ) reflect the properties of the bulk at the so-called kinetic freeze-out, when the momentum distributions are fixed and elastic collisions stopped to occur. The shape of the hadron spectra can be described by an exponential function,

$$E \frac{d^3\sigma}{d^3p_T} \propto e^{-a p_T}, \quad (2.20)$$

where the slope parameter  $a \approx 6 \text{ (GeV}/c)^{-1}$  [21] varies only little with the collision energy. This functional form represents a Boltzmann spectrum of an equilibrated thermal system. Via a more sophisticated model, the so-called Blast-Wave formalism [60], the effective temperature

$$T_{\text{eff}} = T_{\text{Kin}} \cdot \sqrt{\frac{1 + \beta_R}{1 - \beta_R}} \quad (2.21)$$

can be extracted, with  $T_{\text{Kin}}$  as the kinetic freeze-out temperature and  $\beta_R$  as the radial flow velocity. In this model, a superposition of thermal sources is assumed, which are boosted in longitudinal and transverse direction. Hence, the model can be regarded as a simplified version of the hydrodynamical approach to describe the collision evolution. The Blast-Wave function and the effective temperature, the latter is deduced in the limit  $m_T/p_T \rightarrow 1$ , contains the kinetic freeze-out temperature and the radial flow velocity, which describes the boost of the thermal source resulting in a blue-shifted temperature. The functional form of the spectra in this model is given by

$$\frac{dN}{m_T dm_T} \propto \int_0^R r dr m_T I_0 \left( \frac{p_T \sinh \rho}{T_{\text{Kin}}} \right) K_1 \left( \frac{m_T \cosh \rho}{T_{\text{Kin}}} \right), \quad (2.22)$$

where  $m_T = \sqrt{m_0^2 + p_T^2}$  is the transverse mass,  $\rho = \tanh^{-1}(\beta_R)$  denotes the boost angle or rapidity,  $I_0$  and  $K_1$  represent modified Bessel functions.<sup>8</sup> If no radial expansion is present, the formula reduces to

$$\frac{dN}{m_T dm_T} \propto e^{-m_T/T_{\text{Kin}}} \quad \text{for } m_T \gg T_{\text{Kin}}. \quad (2.23)$$

The impact of the boost is visible in the rise of  $R_{AA}$  at  $p_T \approx 2 \text{ GeV}/c$ . If the flow effect was mass (constituent quark number) dependent, one would expect a mass (constituent quark number) dependent enhancement of  $R_{AA}$ . At RHIC, such a mass ordering was indeed observed [61]. To show this at LHC energies is one motivation for this thesis besides the investigation of the high  $p_T$  region.

In addition to the radial flow, which is triggered by the expansion of the source, the so-called elliptic flow acts on the parton momenta in non-central AA collisions. The elliptic flow is a result of a initial spatial azimuthal asymmetry (initial elliptic shape of the over-lap region) relative to the reaction plane resulting in a pressure gradient, which finally causes an anisotropic particle production. The elliptic flow

---

<sup>8</sup>Solution of the Bessel linear differential equation of second order. Modified means here, that the behaviour is exponential instead of oscillating.

is quantified by the parameter<sup>9</sup>  $v_2$  and usually measured as a function of  $p_T$  for different centrality classes and particle species. The largest elliptic flow is observed in mid-central collisions, because here, as compared to peripheral collisions with the strongest asymmetry, the amount of partons is still large enough to transport the pressure. The pressure transport is only possible if a collective behaviour of the medium constituents is given, allowing that the momentum kick from the pressure gradient caused by the spatial anisotropy is imparted among the partons. The fact, that elliptic flow is observed for the final state hadrons, shows, that the thermalisation of the system happens rapidly, i.e. a hydrodynamical system is established before the anisotropy vanishes [20, 64]. Rapid means in this case that  $\tau \lesssim 1 \text{ fm}/c$ , which is much smaller than the system life time of  $\tau \approx 10 \text{ fm}/c$  [65].

The discovery of collectivity and fast thermalisation at RHIC and at the LHC are important findings and an essential input for the EoS. From this review here, flow seems not to be expected in pp collisions—currently it is heavily discussed if pp collisions at LHC energies could built up flow after all. This discussion is triggered by the results of di-hadron correlations in pp, which show as a function of the azimuthal and polar angular difference a similar background profile (a ridge structure on the near-side) as it is observed in Pb–Pb collisions [66]. In the latter system, this structure is thought to be caused by flow. Since in pp collisions at LHC, multiplicities are measured, which are comparable to that of semi-central Pb–Pb collisions, the question of a spacious system in pp—a core—, where collectivity can occur, is reasonable. In [67] a collective hadronisation is suggested and the inclusion of radial flow seems to improve the description of identified hadron spectra in pp [68]. Whether this is the whole answer, remains to be validated within the field.

The above-mentioned Blast-Wave model as a simplified hydrodynamic description is usually used in order to extract the total yield of a particle species since most measured spectra are restricted to a limited  $p_T$  range. For a more system evolution oriented consideration, though, the full hydrodynamic formulation is employed. Within the discussed  $p_T$  range of  $0 \leq p_T \lesssim 3 \text{ GeV}/c$ , the description of the hadron spectra via pure hydrodynamics works reasonably well at RHIC as well as at LHC energies [69, 70].

The hydrodynamical formulation of the system evolution, of the deconfined phase and of the resulting formation of hadron spectra is based on the conservation of the energy-momentum tensor

$$T^{\mu\nu} = (\epsilon + P) u^\mu u^\nu + P \eta^{\mu\nu}, \quad (2.24)$$

with  $P = P(\epsilon)$  as the EoS,  $u^\mu$  the fluid velocity,  $\eta^{\mu\nu}$  the metric tensor, and the baryon number  $B$  via

$$\partial_\mu \langle T^{\mu\nu} \rangle = 0, \quad \partial_\mu \langle j_B^\mu \rangle = 0, \quad (2.25)$$

---

<sup>9</sup>Second component of the Fourier expansion of the azimuthal dependence of the invariant yield [62, 63].

assuming local thermal equilibrium [71]. The latter though, takes a short time to evolve ( $\tau \approx 0.2 - 0.4 \text{ fm}/c$  [64]), which allows the description of the system via a hydro-approach only after the earliest moments of the collision. Hence, the initial conditions (energy density, entropy, net baryon density), as an essential input for the calculations, need to be constrained by measurements, as for example particle multiplicities and transverse energy. From the experimental results for the above-mentioned flow components and those of higher order, matter properties such as the velocity of sound and the viscosity (or shear viscosity, describing the dissipation due to internal friction, over entropy density  $\eta/s$ ) can be extracted. This extraction however is strongly model dependent, since some features, e.g. the energy density profile, do need to be modelled and hence bear a source of systematic uncertainties. From the simulated time evolution, a lower limit of the initial temperature can be deduced, when comparing the calculations to data [72]. Generally it is stated, that the EoS is well constrained by LQCD. The remaining open aspects including the energy density profile, equilibration times, possible pre-equilibrium processes and a possible core-corona separation as well as the exact hadronisation process, though, reflect the uncertainties of the hydrodynamical approach [72, 73].

If a perfect fluid, i.e. a fluid with vanishing viscosity, is considered, the expectation values can be parametrized only by the local energy density,  $\epsilon$ , and the local pressure,  $P$  [71]. The success of viscous hydrodynamical calculations in describing the  $p_T$  spectra as well as the flow components at RHIC and LHC energies has however shown that the medium behaves only approximately as a perfect fluid, approaching closely the lower bound of  $\eta/s = 1/(4\pi) \approx 0.08$  (in units of  $\hbar/k_B$ ) as given by AdS/CFT [74]. This finding adds the viscosity to the parametrisation. For comparison, in case of strongly correlated classical fluids the value is much bigger than  $\hbar/k_B$ , in case of strongly correlated quantum fields however, it is of the order of  $\hbar/k_B$ , “indicating that dissipation is governed by quantum effects” [75] as it is also the case for ultra-cold Fermi gases, which is shown in Fig. 2.11.

That the viscosity indeed matters is shown by the authors of [76], from which Fig. 2.12 is taken. In this figure, the initial energy density as well as the energy density after a system evolution time of 6 fm/c in case of an ideal and a viscous fluid, respectively, are illustrated. Whereas in the ideal case, the initial fluctuations are still somewhat recognizable, the viscosity leads to a significant effect of dissipation. Translating this effect into the calculation of the elliptic flow, it turns out that viscosity reduces the flow effect as compared to the ideal case. This reduction of the flow, which is needed to reproduce the measurements, can be tuned by the value of the viscosity. Recent calculations indicate, that the system at the LHC seems to be “less ideal” than at RHIC [64], where  $\eta/s \approx 0.12$  is 40 % smaller than at LHC energies. Since “a small  $\eta/s$  is generally considered to be evidence for the on-set of a strongly-coupled deconfined plasma early in the evolution of the collision” [77], does a larger value hint to a “weaker” coupled system as it could be expected due to the dependence of  $\alpha_s$  on the energy scale?

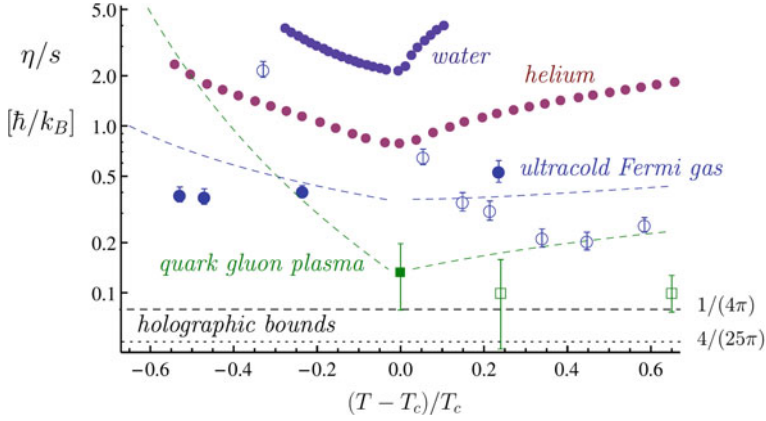


**Fig. 2.11** Transport properties of strongly correlated fluids. The ratio of shear viscosity to entropy density  $s$  as a function of  $(T - T_c)/T_c$ , where  $T_c$  is the super-fluid transition temperature in the case of ultra-cold Fermi gases, the deconfinement temperature in the case of QCD and the critical temperature at the endpoint of the liquid gas transition in the case of water and helium. The QGP point (square) is taken from the analysis of viscous hydrodynamics, the open squares show lattice QCD data and the lattice data for the ultracold Fermi gas are displayed by the open circles. The dashed curves are theory curves. The theories are scaled by overall factors to match the data near  $T_c$ . The lines labelled “holographic bound” correspond to the Kovtun, Son and Starinets (KSS) bound and the Gauss–Bonnet bound (Figure and caption taken from [75].)

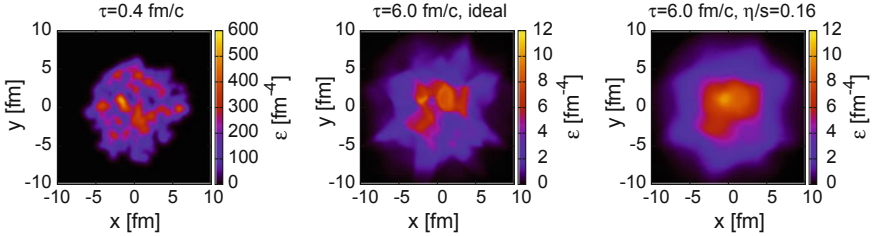


**Fig. 2.12** Energy density distribution in the transverse plane for one event with  $b = 2.4$  fm at the initial time (left), and after  $\tau = 6$  fm/c for the ideal case (middle) and with  $\eta/s = 0.16$  (right). Figure and caption taken from [76]. Calculations from the viscous fluid-dynamic simulation MUSIC

### Baryon-to-Meson-Enhancement

In Fig. 2.13, the proton-to-pion-ratio measured by ALICE is shown for different centralities. In central collisions the ratio exhibits a baryon-to-meson enhancement compared to more peripheral collisions. This enhancement is well described by viscous hydrodynamics for  $p_T \lesssim 3$  GeV/c. Since within the hydrodynamic picture, the collectivity and the flow respectively are the main ingredients, the proton-to-pion ratio can be understood as a result of the mass ordering induced by the radial flow, pushing heavier particles to higher  $p_T$ . In contrast to the anisotropic elliptic flow, the



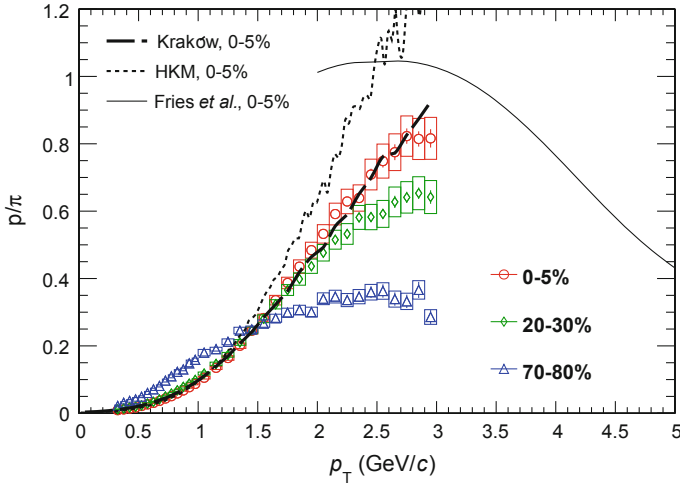


**Fig. 2.13**  $p/\pi = (p + \bar{p})/(\pi^+ + \pi^-)$  as a function of  $p_T$  for different centrality bins compared to ratios from the Kraków [78] and HKM [79] hydrodynamic models and to a recombination model [80]. Figure and caption taken from [69]

radial flow is strongest in central collisions and increases with collision energy if the same centralities are considered [69].

Leaving the hydro-regime and regarding now the momentum region above, another hadron production mechanism or the hadron production influencing mechanism may come into effect. The authors of [80] propose “that hadron production at momenta of a few GeV/c in an environment with a high density of partons occurs by recombination, rather than fragmentation, of partons.” It is shown “that recombination always dominates over fragmentation for an exponentially falling parton spectrum, but that fragmentation wins out eventually, when the spectrum takes the form of a power-law.” Recombination means in this case that baryons and mesons are formed within a densely populated phase space from combinations of the available quarks and anti-quarks during the hadronisation process, i.e. at a late stage of the system evolution. Since the population in the lower  $p_T$  region is much larger than at higher  $p_T$  due to the steeply falling parton spectrum, the recombination is expected to appear mainly at low  $p_T$ . The low phase space density at high  $p_T$  seems to suppress the recombination, although it is principally much easier to build a high  $p_T$  hadron from three quarks with momenta of  $p_T/3$  than from a fragmenting parton which needs to have a much higher  $p_T$  than the resulting hadron. Two basic features characterize the recombination model: ‘the probability for the emission of a meson (baryon) is proportional to the single parton distribution squared (cubed), and the parton momenta sum up to the hadron momentum’ [80].

Concerning the elliptic flow  $v_2$ , in the recombination picture this quantity should not scale with the particle mass but rather obey the quark number scaling. The latter is given if the  $v_2$  distributions of different particles fall on a single curve when  $v_2$

and the corresponding  $p_T$  are divided by the number of constituent quarks. At RHIC, such a scaling was indeed observed, though at the LHC, it is violated by  $\approx 20\%$  [81]. As a remark, in case of RHIC, the key measurement for the idea of constituent quark number scaling was the  $v_2$  and the  $R_{AA}$  of the  $\phi$  meson, which has a slightly larger mass than a proton but shows a similar  $v_2$  and suppression as the pions [61]. Regarding the particle production in central collisions, baryons should hence profit more from the radial partonic flow than mesons, because baryons consist of three quarks whose  $p_T$  were shifted to higher values. Consequently, in the recombination picture, an enhancement of the baryon-to-meson ratio could be expected for central collisions, where the radial flow is largest. Therefore, the observed baryon-to-meson enhancement in central collisions at RHIC [61, 82, 83] could be interpreted in terms of recombination at intermediate  $p_T$ . Comparisons of model calculations with data from RHIC show an agreement up to  $p_T \approx 5 \text{ GeV}/c$  [83].

Is recombination also given at the LHC? When does fragmentation take over? This discussion is left to the last chapter of this document.

## 2.3 Modification of $K_s^0$ and $\Lambda(\bar{\Lambda})$ $p_T$ Spectra in Pb–Pb Collisions

The  $K_s^0$  meson and the  $\Lambda(\bar{\Lambda})$  baryon are particles containing strange quarks. Prior to the review of the thesis title and its motivation, the role of strangeness in heavy-ion collisions is discussed in the following.

### 2.3.1 *What a Strange Particle!—Strangeness in AA Collisions*

“The very high abundance of strange particles, in particular of hyperons (the Omega-to-pion ratio increases by up to a factor 20 from pp to Pb–Pb), was predicted as a consequence of QGP formation. Today it is interpreted more generally as a manifestation of statistical hadronisation from a thermalised medium, where most hadrons, not only those containing strange quarks, are created in thermal equilibrium ratios” [84].

Strange particles are those particles, which consist of at least one  $s$  ( $\bar{s}$ ) quark. In case of strange baryons, one also speaks about hyperons. The particles analysed ( $\Lambda$ ,  $K_s^0$ ) or regarded in this work are listed in Table 2.1. In case of the baryons, also the anti-particles with opposite charge as well as the corresponding anti-quark content and the anti-decay-particles are considered, which are not included in the table.

The occurrence of strangeness is dominated by the production from fragmentation and string breaking as compared to the availability as sea-quarks in the nucleons determined by the PDFs. Simply speaking, strangeness needs to be produced during

**Table 2.1** Strange particles analysed or regarded in this work

Particle	Mass (GeV/ $c^2$ )	Quark content	Decay channel	BR (%)	$c\tau$ (cm)
<b>Baryons</b>					
$\Lambda$	1.115	uds	$p + \pi^-$	63.9	7.89
$\Xi^-$	1.321	dss	$\Lambda + \pi^-$	99.9	4.91
$\Xi^0$	1.314	uss	$\Lambda + \pi^0$	99.5	8.7
$\Omega^-$	1.672	sss	$\Lambda + K^-$	67.8	2.46
<b>Mesons</b>					
$K_s^0$	0.498	$\frac{1}{\sqrt{2}}(d\bar{s} + \bar{d}s)$	$\pi^+ + \pi^-$	69.2	2.68
$K^+$	0.494	$u\bar{s}$	$\mu^+ + \nu_\mu$	63.6	371
$K^-$	0.494	$\bar{u}s$	$\mu^- + \nu_{\bar{\mu}}$	69.2	371

BR: branching ratio,  $c\tau$ : mean proper decay length. Values from [14]

the collision in contrast to u and d quarks, which are present as valence quarks at the initial state. The dominant mechanism is the gluon fusion with  $gg \rightarrow s\bar{s}$ . Quark-anti-quark annihilation is suppressed, because the time scale is too long as compared to the QGP equilibrium and to the gluon fusion.

In central AA collisions, where a thermal equilibrated state is likely to be formed, also statistical equilibration is thought to be reached. Statistical equilibration is produced in a “system of hadrons of given energy, baryon number and strangeness from some non-hadronic state by a statistical process, which fills hadronic phase-space in the statistically most probable configuration” [85]. Since strangeness is conserved by the strong interaction, s and  $\bar{s}$  quarks have to be produced by the same amount. Hence, in small systems, together with one strange hadron, another hadron with opposite strangeness has to be created inside the small volume at the same time. The latter requires more energy as compared to heavy-ion collisions, limiting the production rate: In AA collisions, the strangeness conservation needs to be fulfilled only globally, because the production of a strange hadron can be compensated by the production of an anti-strange hadron on the other side of the nuclear fireball [85]—the larger phase space relaxes the local strangeness conservation. Whereas pp and peripheral AA collisions can be regarded as canonical systems, central AA collisions rather represent a grand canonical ensemble [86]. Consequently, one speaks about canonical suppression of strangeness in pp collisions as compared to AA collisions.

The strange hadrons profiting most from the strangeness re-distribution within the system are the multi-strange hadrons such as  $\Xi$  and  $\Omega$ . In Fig. 2.14a, b, the ratio of the abundances of these particles from pp to central heavy-ion collisions are shown as a function of  $N_{\text{part}}$  for SPS, RHIC and LHC energies. The ratios are normalised to  $N_{\text{part}}$  in order to account for the system size. The observed strangeness suppression, represented by the ratios all exceeding unity, is increasing with decreasing collision energies. In case of the  $\Omega^-$ , the values are larger than for  $\Xi^-$  at all energies, which could be a result of the triple s quark content of the  $\Omega^-$  reflecting the enhanced  $s\bar{s}$  in a hot and extended medium.

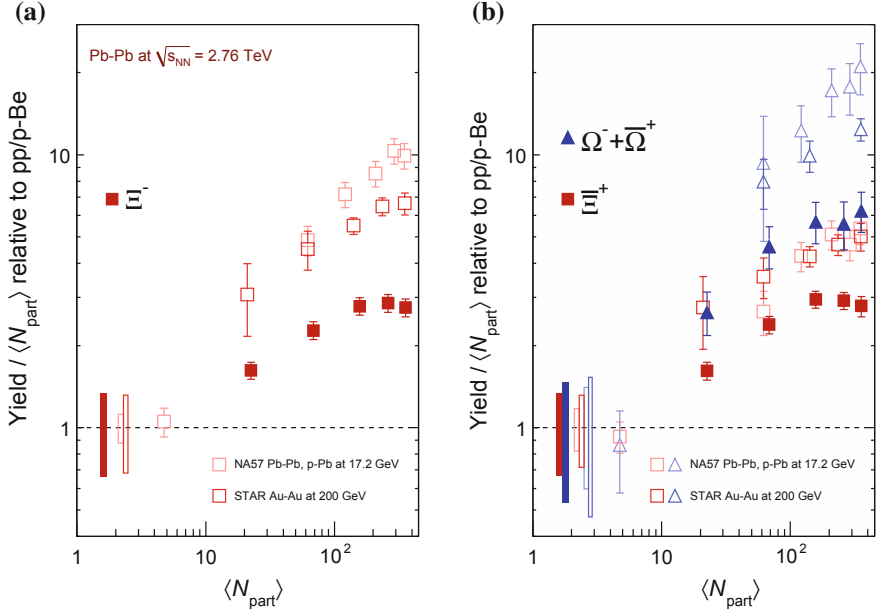


**Fig. 2.14** Enhancements in the rapidity range  $|y| < 0.5$  as a function of the mean number of participants  $\langle N_{\text{part}} \rangle$ , showing LHC (ALICE, *full symbols*), RHIC and SPS (*open symbols*) data. The LHC data use interpolated pp values (see text). *Boxes on the dashed line at unity* indicate statistical and systematic uncertainties on the pp or pBe reference. *Error bars* on the data points represent the corresponding uncertainties for all the heavy-ion measurements and those for p-Pb at the SPS. Figure and caption taken from [70]

Apart from the multi-strange baryon production, also the abundances of single strange particles are of interest. Within this work, additionally the production of single strange particles as compared to pp and to pions is addressed.

As soon as the mean free path of the elastic reactions becomes larger than the system size as a consequence of the expansion, the thermal equilibrium collapses and the system freezes out. This freeze-out reflects the already mentioned kinetic freeze-out. Prior to that, the system is anticipated to freeze-out chemically, i.e. the thermal equilibrium is maintained, but the hadron abundances are fixed due to the vanishing inelastic reactions [71]. Thus, the chemical freeze-out is expected to occur at a higher temperature  $T_{\text{ch}}$  than the kinetic freeze-out. Therefore, in order to obtain a full description of the particle production from a hydrodynamical consideration, the calculation of the hydrodynamical phase must be followed by a hadronic freeze-out formalism including the freeze-out stage(s). The assumption of their duration as well as of the chemical freeze-out existence and its temperature are the main source of large systematic uncertainties of the calculations.

The following parameters mainly describing the particle production in equilibrium are  $T_{\text{ch}}$ ,  $\mu_B$  via the ratio of the  $\bar{p}/p$  yield,

$$\frac{\bar{p}}{p} = e^{\frac{-2\mu_B}{T_{\text{ch}}}}, \quad (2.26)$$

and the volume  $V$ , that is typically constrained by the pion production, as a normalization parameter [87]. Statistical hadronisation models (SHM) are relatively successful in describing particle abundances and the corresponding particle ratios. The chemical freeze-out temperature is obtained from a global fit to a large number of different particle yields. Current estimates are  $T_{\text{ch}} = 156 \text{ MeV}$  ( $\mu_B = 0$ ) in [88] and  $T_{\text{ch}} 170 \text{ MeV}$  ( $\mu_B = 1 \text{ MeV}$ ) in [89]. These models, as mentioned at the beginning of this section, assume a thermally equilibrated, grand-canonical system, that finally freezes out after the creation of hadrons. The hadronisation process is described by the formation of massive colourless objects such as clusters. “Each cluster gives rise to multi-hadronic states in a purely statistical fashion” [90], which means that the formalism for statistical ensembles are used to extract information, such as the chemical freeze-out temperature, from the clusters. Most of the SHM models additionally contain the so-called strangeness suppression factor  $\gamma_s$ , which is 0.5–0.7 in elementary collisions and  $\approx 1$  in non-peripheral heavy-ion collisions.

Closing questions are: How is the thermal equilibrium established? How is the chemical and the kinetic freeze-out reached; are they universal? Does a chemical freeze-out exist or is there only one freeze-out stage? These aspects are still under investigation. Two competing scenarios for the equilibrium are discussed in [84]: The system is either evolving into (thermal) equilibrium or the partons are born into (phase-space) equilibrium [91]. It has to be clarified, “whether it is a proper thermal-statistical equilibrium in a finite volume or rather a phase space dominance effect” [92]. The authors of [93] argue that the chemical freeze-out is indeed given by a universal statistical hadronisation. While the latest temperature of chemical equilibrium is expected to be universal and to coincide with the critical (cross-over) temperature from LQCD,  $T_{\text{ch}}$  is found to be centrality-dependent. On the other hand, since the chemical freeze-out temperature resembles the QCD temperature, doubts exist, that the chemical freeze-out takes place at all or at least appears as a separate stage of the collision.

### 2.3.2 $R_{\text{AA}}$ of $K_s^0$ and $\Lambda(\bar{\Lambda})$

Summarising this chapter, the working title of this thesis, “Modification of  $K_s^0$  and  $\Lambda(\bar{\Lambda})$   $p_T$  spectra in Pb–Pb collisions with ALICE”, adds two further dimensions to the initial problem statement as discussed at the beginning: Could an AA collision be understood as a superposition of single pp collisions?

During the last sections it was argued that AA collisions are not comparable with a pp superposition picture, neither at high nor at low  $p_T$ . At high  $p_T$ , the fragmentation

and/or the energy loss in the medium cause the difference, while at low  $p_T$ , different strangeness production mechanisms are at work. In case of flow, the situation in pp seems to be less clear, but flow is in fact considered to be strongest in Pb–Pb collisions.

The additional dimensions as further means for exploring possible differences of the two collision systems, here, are the strangeness on the one hand and the baryon-versus-meson comparison on the other. The advantage of  $K_s^0$  and  $\Lambda(\bar{\Lambda})$  as compared to the multi-strange particles is given by their larger  $p_T$  reach, enabling the study of the high  $p_T$  region, where the fragmentation and the parton energy loss are the aspects of interest. The low  $p_T$  region is investigated in order to quantify the strangeness production and to investigate the balance of different particle production mechanisms in the two collision systems. The main research questions of this work are:

- How does the  $R_{AA}$  of  $K_s^0$  and  $\Lambda(\bar{\Lambda})$  compare to that of unidentified charged particles?
- Is the modification different for different flavours?
- Are there divergences for baryons and mesons?
- Is the modification different for particles and anti-particles?
- How does the modification change, when comparing to lower collision energies?
- How much strangeness is produced in pp at the LHC?

For addressing these questions, the  $p_T$  spectra of  $K_s^0$  and  $\Lambda(\bar{\Lambda})$  are determined in pp collisions as well as for different centralities in Pb–Pb collisions. The adjacent chapter reviews the experimental conditions, the data analysis is then discussed in the subsequent chapter.

## References

1. X.-N. Wang, Effects of jet quenching on high  $p_T$  hadron spectra in highenergy nuclear collisions. *Phys. Rev. C* **58**, 2321 (1998). doi:[10.1103/PhysRevC.58.2321](https://doi.org/10.1103/PhysRevC.58.2321)
2. A. Andronic, An overview of the experimental study of quark-gluon matter in high-energy nucleus-nucleus collisions. *Int. J. Mod. Phys. A* **29**, 1430047 (2014). doi:[10.1142/S0217751X14300476](https://doi.org/10.1142/S0217751X14300476)
3. K. Aamodt et al., Centrality dependence of the charged-particle multiplicity density at midrapidity in Pb-Pb collisions at  $\sqrt{s_{NN}} = 2.76$  TeV. *Phys. Rev. Lett.* **106**, 032301 (2011). doi:[10.1103/PhysRevLett.106.032301](https://doi.org/10.1103/PhysRevLett.106.032301)
4. B. Back et al., Centrality dependence of charged hadron transverse momentum spectra in Au-Au collisions from  $\sqrt{s_{NN}} = 62.4$  to 200 GeV. *Phys. Rev. Lett.* **94**, 082304 (2005). doi:[10.1103/PhysRevLett.94.082304](https://doi.org/10.1103/PhysRevLett.94.082304)
5. J.D. Bjorken, Energy loss of energetic partons in quark - gluon plasma: possible extinction of high  $p(t)$  jets in hadron - hadron collisions, FERMILAB-PUB-82-059-THY (1982)
6. M. Gyulassy, M. Plümer, Jet quenching in dense matter. *Phys. Lett. B* **243**, 432 (1990). doi:[10.1016/0370-2693\(90\)91409-5](https://doi.org/10.1016/0370-2693(90)91409-5)
7. B. Abelev et al., Centrality dependence of charged particle production at large transverse momentum in Pb-Pb collisions at  $\sqrt{s_{NN}} = 2.76$  TeV. *Phys. Lett. B* **720**, 52 (2013). doi:[10.1016/j.physletb.2013.01.051](https://doi.org/10.1016/j.physletb.2013.01.051)

8. G.I. Veres, Overview of results on jets from the CMS collaboration. Nucl. Phys. A **904–905**, 146c (2013). doi:[10.1016/j.nuclphysa.2013.01.056](https://doi.org/10.1016/j.nuclphysa.2013.01.056)
9. T. Renk, Towards jet tomography:  $\gamma$ -hadron correlations. Phys. Rev. C **74**, 034906 (2006). doi:[10.1103/PhysRevC.74.034906](https://doi.org/10.1103/PhysRevC.74.034906)
10. R.P. Feynman, Very high-energy collisions of hadrons. Phys. Rev. Lett. **23**, 1415 (1969). doi:[10.1103/PhysRevLett.23.1415](https://doi.org/10.1103/PhysRevLett.23.1415)
11. R.P. Feynman, *Photon-Hadron Interactions* (WA Benjamin Inc, Reading, 1972)
12. J.D. Bjorken, Can we measure parton-parton cross sections? Phys. Rev. D **8**, 4098 (1973). doi:[10.1103/PhysRevD.8.4098](https://doi.org/10.1103/PhysRevD.8.4098)
13. J.F. Owens, Large-momentum-transfer production of direct photons, jets, and particles. Rev. Mod. Phys. **59**, 465 (1987). doi:[10.1103/RevModPhys.59.465](https://doi.org/10.1103/RevModPhys.59.465)
14. K. Olive et al., Review of particle physics. Chin. Phys. C **38**, 090001 (2014). <http://pdg.lbl.gov/>
15. I.J. Aitchison, A.J. Hey, *Gauge Theories in Particle Physics*, vol. 2, 4th edn. (CRC Press, Boca Raton, 2012)
16. Y.L. Dokshitzer, Calculation of the structure functions for deep inelastic scattering and  $e^+e^-$  annihilation by perturbation theory in quantum chromodynamics. Sov. Phys. JETP **46**, 641 (1977)
17. V. Gribov, L. Lipatov, Deep inelastic  $e$ - $p$  scattering in perturbation theory. Sov. J. Nucl. Phys. **15**, 438 (1972)
18. L. Lipatov, The parton model and perturbation theory. Sov. J. Nucl. Phys. **20**, 94 (1975)
19. G. Altarelli, G. Parisi, Asymptotic freedom in parton language. Nucl. Phys. B **126**, 298 (1977). doi:[10.1016/0550-3213\(77\)90384-4](https://doi.org/10.1016/0550-3213(77)90384-4)
20. J. Rak, M.J. Tannenbaum, *High  $p_T$  Physics in the Heavy Ion Era* (Cambridge University Press, Cambridge, 2013)
21. S.M. Berman, J.D. Bjorken, J.B. Kogut, Inclusive processes at high transverse momentum. Phys. Rev. D **4**, 3388 (1971). doi:[10.1103/PhysRevD.4.3388](https://doi.org/10.1103/PhysRevD.4.3388)
22. B.B. Abelev et al., Energy dependence of the transverse momentum distributions of charged particles in  $pp$  collisions measured by ALICE. Eur. Phys. J. C **73**, 2662 (2013). doi:[10.1140/epjc/s10052-013-2662-9](https://doi.org/10.1140/epjc/s10052-013-2662-9)
23. K.J. Eskola, H. Paukkunen, C.A. Salgado, Nuclear PDFs at NLO - status report and review of the EPS09 results. Nucl. Phys. A **855**, 150 (2011). doi:[10.1016/j.nuclphysa.2011.02.032](https://doi.org/10.1016/j.nuclphysa.2011.02.032)
24. K.J. Eskola, H. Paukkunen, C.A. Salgado, EPS09 - A new generation of NLO and LO nuclear parton distribution functions. JHEP **2009**, 065 (2009). <http://stacks.iop.org/1126-6708/2009/i=04/a=065>
25. S. Albino, B. Kniesl, G. Kramer, AKK update: improvements from new theoretical input and experimental data. Nucl. Phys. B **803**, 42 (2008). doi:[10.1016/j.nuclphysb.2008.05.017](https://doi.org/10.1016/j.nuclphysb.2008.05.017)
26. D. d'Enterria, Relativistic heavy ion physics: 6.4 jet quenching, in *Springer Materials - Landolt-Bornstein - Group I elementary Particles, Nuclei and Atoms*, vol. 23, ed. by R. Stock (Springer, New York, 2010). doi:[10.1007/978-3-642-01539-7\\_16](https://doi.org/10.1007/978-3-642-01539-7_16)
27. Y. Dokshitzer, D. Kharzeev, Heavy-quark colorimetry of QCD matter. Phys. Lett. B **519**, 199 (2001). doi:[10.1016/S0370-2693\(01\)01130-3](https://doi.org/10.1016/S0370-2693(01)01130-3)
28. M. Nahrgang et al., Azimuthal correlations of heavy quarks in Pb-Pb collisions at  $\sqrt{s} = 2.76$  TeV at the CERN large hadron collider. Phys. Rev. C **90**, 024907 (2014). doi:[10.1103/PhysRevC.90.024907](https://doi.org/10.1103/PhysRevC.90.024907)
29. B. Zakharov, Fully quantum treatment of the Landau-Pomeranchuk-Migdal effect in QED and QCD. JETP Lett. **63**, 952 (1996). doi:[10.1134/1.567126](https://doi.org/10.1134/1.567126)
30. S. Wicks et al., Elastic, inelastic, and path length fluctuations in jet tomography. Nucl. Phys. A **784**, 426 (2007). doi:[10.1016/j.nuclphysa.2006.12.048](https://doi.org/10.1016/j.nuclphysa.2006.12.048)
31. T. Renk, Constraining the physics of jet quenching. Phys. Rev. C **85**, 044903 (2012). doi:[10.1103/PhysRevC.85.044903](https://doi.org/10.1103/PhysRevC.85.044903)
32. T. Renk, Physics probed by the  $p_T$  dependence of the nuclear suppression factor. Phys. Rev. C **88**, 014905 (2013). doi:[10.1103/PhysRevC.88.014905](https://doi.org/10.1103/PhysRevC.88.014905)

33. K. Aamodt et al., Particle-yield modification in jet-like azimuthal di-hadron correlations in Pb-Pb collisions at  $\sqrt{s_{NN}} = 2.76$  TeV. Phys. Rev. Lett. **108**, 092301 (2012). doi:[10.1103/PhysRevLett.108.092301](#)
34. B. Abelev et al., Parton energy loss in heavy-ion collisions via direct-photon and charged-particle azimuthal correlations. Phys. Rev. C **82**, 034909 (2010). doi:[10.1103/PhysRevC.82.034909](#)
35. A. Adare et al., Trends in yield and azimuthal shape modification in dihadron correlations in relativistic heavy ion collisions. Phys. Rev. Lett. **104**, 252301 (2010). doi:[10.1103/PhysRevLett.104.252301](#)
36. B. Betz, M. Gyulassy, Examining a reduced jet-medium coupling in Pb-Pb collisions at the large hadron collider. Phys. Rev. C **86**, 024903 (2012). doi:[10.1103/PhysRevC.86.024903](#)
37. M. van Leeuwen, Lectures at Helmholtz Graduate School, 28 Feb–5 March, Manigod, France (2011). <http://www.staff.science.uu.nl/~leeuw179/>
38. S.S. Adler et al., Detailed study of high- $p_T$  neutral pion suppression and azimuthal anisotropy in Au-Au collisions at  $\sqrt{s_{NN}} = 200$  GeV. Phys. Rev. C **76**, 034904 (2007). doi:[10.1103/PhysRevC.76.034904](#)
39. B. Abelev et al., Measurement of the inclusive differential jet cross section in pp collisions at  $\sqrt{s} = 2.76$  TeV. Phys. Lett. B **722**, 262 (2013). doi:[10.1016/j.physletb.2013.04.026](#)
40. A. Adare et al., Neutral pion production with respect to centrality and reaction plane in Au-Au collisions at  $\sqrt{s_{NN}} = 200$  GeV. Phys. Rev. C **87**, 034911 (2013). doi:[10.1103/PhysRevC.87.034911](#)
41. K. Aamodt et al., Suppression of charged particle production at large transverse momentum in central Pb-Pb collisions at  $\sqrt{s_{NN}} = 2.76$  TeV. Phys. Lett. B **696**, 30 (2011). doi:[10.1016/j.physletb.2010.12.020](#)
42. D. Kharzeev, Parton energy loss at strong coupling and the universal bound. Eur. Phys. J. C **61**, 675 (2009). doi:[10.1140/epjc/s10052-008-0860-7](#)
43. S. Chatrchyan et al., Study of high- $p_T$  charged particle suppression in Pb-Pb compared to pp collisions at  $\sqrt{s_{NN}} = 2.76$  TeV. Eur. Phys. J. C **72**, 1945 (2012). doi:[10.1140/epjc/s10052-012-1945-x](#)
44. T. Renk et al., Systematics of the charged-hadron  $p_T$  spectrum and the nuclear suppression factor in heavy-ion collisions from  $\sqrt{s_{NN}} = 200$  GeV to  $\sqrt{s_{NN}} = 2.76$  TeV. Phys. Rev. C **84**, 014906 (2011). doi:[10.1103/PhysRevC.84.014906](#)
45. M. Gyulassy, P. Levai, I. Vitev, Jet quenching in thin quark gluon plasmas I: formalism. Nucl. Phys. B **571**, 197 (2000). doi:[10.1016/S0550-3213\(99\)00713-0](#)
46. M. Gyulassy, P. Levai, I. Vitev, Reaction operator approach to nonabelian energy loss. Nucl. Phys. B **594**, 371 (2001). doi:[10.1016/S0550-3213\(00\)00652-0](#)
47. C.A. Salgado, U.A. Wiedemann, Calculating quenching weights. Phys. Rev. D **68**, 014008 (2003). doi:[10.1103/PhysRevD.68.014008](#)
48. P.B. Arnold, G.D. Moore, L.G. Yaffe, Photon and gluon emission in relativistic plasmas. JHEP **0206**, 030 (2002). doi:[10.1088/1126-6708/2002/06/030](#)
49. X.-N. Wang, X. Guo, Multiple parton scattering in nuclei: parton energy loss. Nucl. Phys. A **696**, 788 (2001). doi:[10.1016/S0375-9474\(01\)01130-7](#)
50. X.-F. Chen et al., Suppression of high- $p_T$  hadrons in Pb-Pb collisions at energies available at the CERN large hadron collider. Phys. Rev. C **84**, 034902 (2011). doi:[10.1103/PhysRevC.84.034902](#)
51. A. Majumder, B. Müller, Hadron mass spectrum from lattice QCD. Phys. Rev. Lett. **105**, 252002 (2010). doi:[10.1103/PhysRevLett.105.252002](#)
52. T. Renk, Path-length dependence of energy loss within in-medium showers. Phys. Rev. C **83**, 024908 (2011). doi:[10.1103/PhysRevC.83.024908](#)
53. W. Horowitz, M. Gyulassy, Heavy quark jet tomography of Pb-Pb at LHC: AdS/CFT drag or pQCD energy loss? Phys. Lett. B **666**, 320 (2008). doi:[10.1016/j.physletb.2008.04.065](#)
54. T. Renk, Charm energy loss and D-D correlations from a shower picture. Phys. Rev. C **89**, 054906 (2014). doi:[10.1103/PhysRevC.89.054906](#)



55. A. Majumder, M. Van Leeuwen, The theory and phenomenology of perturbative QCD based jet quenching. *Prog. Part. Nucl. Phys. A* **66**, 41 (2011). doi:[10.1016/j.pnpnp.2010.09.001](https://doi.org/10.1016/j.pnpnp.2010.09.001)
56. B.A. Kniehl, G. Kramer, B. Potter, Testing the universality of fragmentation functions. *Nucl. Phys. B* **597**, 337 (2001). doi:[10.1016/S0550-3213\(00\)00744-6](https://doi.org/10.1016/S0550-3213(00)00744-6)
57. T. Matsui, H. Satz,  $J/\psi$  suppression by quark-gluon plasma formation. *Phys. Lett. B* **178**, 416 (1986). doi:[10.1016/0370-2693\(86\)91404-8](https://doi.org/10.1016/0370-2693(86)91404-8)
58. T. Renk, K.J. Eskola, Proton-antiproton suppression in 200A GeV Au-Au collisions. *Phys. Rev. C* **76**, 027901 (2007). doi:[10.1103/PhysRevC.76.027901](https://doi.org/10.1103/PhysRevC.76.027901)
59. J. Aichelin, P.B. Gossiaux, T. Gousset, Gluon radiation by heavy quarks at intermediate energies. *Phys. Rev. D* **89**, 074018 (2014). doi:[10.1103/PhysRevD.89.074018](https://doi.org/10.1103/PhysRevD.89.074018)
60. E. Schnedermann, J. Sollfrank, U. Heinz, Thermal phenomenology of hadrons from 200A GeV S+S collisions. *Phys. Rev. C* **48**, 2462 (1993). doi:[10.1103/PhysRevC.48.2462](https://doi.org/10.1103/PhysRevC.48.2462)
61. S.S. Adler et al., Production of  $\phi$  mesons at midrapidity in  $\sqrt{s_{NN}} = 200$  GeV. *Phys. Rev. C* **72**, 014903 (2005). doi:[10.1103/PhysRevC.72.014903](https://doi.org/10.1103/PhysRevC.72.014903)
62. S. Voloshin, Y. Zhang, Flow study in relativistic nuclear collisions by Fourier expansion of Azimuthal particle distributions. *Z. Phys. C* **70**, 665 (1996). doi:[10.1007/s002880050141](https://doi.org/10.1007/s002880050141)
63. J.-Y. Ollitrault, Anisotropy as a signature of transverse collective flow. *Phys. Rev. D* **46**, 229 (1992). doi:[10.1103/PhysRevD.46.229](https://doi.org/10.1103/PhysRevD.46.229)
64. C. Gale et al., Event-by-event anisotropic flow in heavy-ion collisions from combined Yang-Mills and viscous fluid dynamics. *Phys. Rev. Lett.* **110**, 012302 (2013). doi:[10.1103/PhysRevLett.110.012302](https://doi.org/10.1103/PhysRevLett.110.012302)
65. K. Aamodt et al., Two-pion Bose-Einstein correlations in central Pb-Pb collisions at  $\sqrt{s_{NN}} = 2.76$  TeV. *Phys. Lett. B* **696**, 328 (2011). doi:[10.1016/j.physletb.2010.12.053](https://doi.org/10.1016/j.physletb.2010.12.053)
66. V. Khachatryan et al., Observation of long-range near-side angular correlations in proton-proton collisions at the LHC. *JHEP* **1009**, 091 (2010). doi:[10.1007/JHEP09\(2010\)091](https://doi.org/10.1007/JHEP09(2010)091)
67. T. Pierog et al., EPOS LHC: test of collective hadronization with LHC data (2013). [arXiv:1306.0121](https://arxiv.org/abs/1306.0121) [hep-ph]
68. K. Werner et al., Analysing radial flow features in p-Pb and p-p collisions at several TeV by studying identified particle production in EPOS3. *Phys. Rev. C* **89**, 064903 (2014). doi:[10.1103/PhysRevC.89.064903](https://doi.org/10.1103/PhysRevC.89.064903)
69. B. Abelev et al., Centrality dependence of  $\pi$ , K, p production in Pb-Pb collisions at  $\sqrt{s_{NN}} = 2.76$  TeV. *Phys. Rev. C* **88**, 044910 (2013). doi:[10.1103/PhysRevC.88.044910](https://doi.org/10.1103/PhysRevC.88.044910)
70. B. Abelev et al., Multi-strange baryon production at mid-rapidity in Pb-Pb collisions at  $\sqrt{s_{NN}} = 2.76$  TeV. *Phys. Lett. B* **728**, 216 (2014). doi:[10.1016/j.physletb.2013.11.048](https://doi.org/10.1016/j.physletb.2013.11.048)
71. T. Hatsuda, K. Yagi, Y. Miake, *Quark-Gluon Plasma* (Cambridge University Press, Cambridge, 2005)
72. B. Müller, Investigation of hot QCD matter: theoretical aspects (2013). [arXiv:1309.7616](https://arxiv.org/abs/1309.7616) [nucl-th]
73. M. Nahrgang et al., Elliptic and triangular flow of heavy flavor in heavy-ion collisions. *Phys. Rev. C* **91**, 014904 (2015). doi:[10.1103/PhysRevC.91.014904](https://doi.org/10.1103/PhysRevC.91.014904)
74. P. Kovtun, D.T. Son, A.O. Starinets, Viscosity in strongly interacting quantum field theories from black hole physics. *Phys. Rev. Lett.* **94**, 111601 (2005). doi:[10.1103/PhysRevLett.94.111601](https://doi.org/10.1103/PhysRevLett.94.111601)
75. A. Adams et al., Strongly correlated quantum fluids: ultracold quantum gases, quantum chromodynamic plasmas and holographic duality. *New J. Phys.* **14**, 115009 (2012). doi:[10.1088/1367-2630/14/11/115009](https://doi.org/10.1088/1367-2630/14/11/115009)
76. B. Schenke, S. Jeon, C. Gale, Elliptic and triangular flow in event-by-event  $D = 3 + 1$  viscous hydrodynamics. *Phys. Rev. Lett.* **106**, 042301 (2011). doi:[10.1103/PhysRevLett.106.042301](https://doi.org/10.1103/PhysRevLett.106.042301)
77. H. Song et al., 200 A GeV Au-Au collisions serve a nearly perfect quarkgluon liquid. *Phys. Rev. Lett.* **106**, 192301 (2011). doi:[10.1103/PhysRevLett.106.192301](https://doi.org/10.1103/PhysRevLett.106.192301)
78. P. Bozek, I. Wyskiel-Piekarska, Particle spectra in Pb-Pb collisions at  $\sqrt{s_{NN}} = 2.76$  TeV. *Phys. Rev. C* **85**, 064915 (2012). doi:[10.1103/PhysRevC.85.064915](https://doi.org/10.1103/PhysRevC.85.064915)
79. I.A. Karpenko, Y.M. Sinyukov, K. Werner, Uniform description of bulk observables in the hydrokinetic model of AA collisions at the BNL relativistic heavy ion collider and the CERN large hadron collider. *Phys. Rev. C* **87**, 024914 (2013). doi:[10.1103/PhysRevC.87.024914](https://doi.org/10.1103/PhysRevC.87.024914)

80. R.J. Fries et al., Hadronization in heavy-ion collisions: recombination and fragmentation of partons. *Phys. Rev. Lett.* **90**, 202303 (2003). doi:[10.1103/PhysRevLett.90.202303](https://doi.org/10.1103/PhysRevLett.90.202303)
81. B.B. Abelev et al., Elliptic flow of identified hadrons in Pb-Pb collisions at  $\sqrt{s_{NN}} = 2.76$  TeV (2014). [arXiv:1405.4632](https://arxiv.org/abs/1405.4632) [nucl-ex]
82. S. Adler et al., Scaling properties of proton and anti-proton production in  $\sqrt{s_{NN}} = 200$  GeV Au-Au collisions. *Phys. Rev. Lett.* **91**, 172301 (2003). doi:[10.1103/PhysRevLett.91.172301](https://doi.org/10.1103/PhysRevLett.91.172301)
83. B. Abelev et al., Energy dependence of  $\pi^{+,-}$ , p and anti-p transverse momentum spectra for Au-Au collisions at  $\sqrt{s_{NN}} = 62.4$  and 200 GeV. *Phys. Lett. B* **655**, 104 (2007). doi:[10.1016/j.physletb.2007.06.035](https://doi.org/10.1016/j.physletb.2007.06.035)
84. J. Schukraft, Heavy ion physics at the LHC: What's new? What's next? (2013). [arXiv:1311.1429](https://arxiv.org/abs/1311.1429) [hep-ex]
85. U.W. Heinz, Concepts of heavy ion physics (2004), pp. 165–238. [arXiv:hep-ph/0407360](https://arxiv.org/abs/hep-ph/0407360) [hep-ph]
86. P. Braun-Munzinger, K. Redlich, J. Stachel, Particle production in heavy ion collisions (2003). [arXiv:nuc1-th/0304013](https://arxiv.org/abs/nuc1-th/0304013) [nucl-th]
87. M. Floris, Hadron yields and the phase diagram of strongly interacting matter. *Nucl. Phys. A* **931**, 103 (2014). doi:[10.1016/j.nuc1physa.2014.09.002](https://doi.org/10.1016/j.nuc1physa.2014.09.002)
88. J. Stachel et al., Confronting LHC data with the statistical hadronization model. *J. Phys. Conf. Ser.* **509**, 012019 (2014). doi:[10.1088/1742-6596/509/1/012019](https://doi.org/10.1088/1742-6596/509/1/012019)
89. J. Cleymans et al., Statistical model predictions for particle ratios at  $\sqrt{s_{NN}} = 5.5$  TeV. *Phys. Rev. C* **74**, 034903 (2006). doi:[10.1103/PhysRevC.74.034903](https://doi.org/10.1103/PhysRevC.74.034903)
90. F. Becattini, R. Fries, The QCD confinement transition: hadron formation. *Landolt-Bornstein* **23**, 208 (2010). doi:[10.1007/978-3-642-01539-7\\_8](https://doi.org/10.1007/978-3-642-01539-7_8)
91. R. Hagedorn, CERN lectures thermodynamics of strong interactions, CERN Publications, European Organisation for Nuclear Research (1970–1971)
92. F. Becattini, An Introduction to the statistical hadronization model (2009). [arXiv:0901.3643](https://arxiv.org/abs/0901.3643) [hep-ph]
93. F. Becattini et al., Centrality dependence of hadronization and chemical freeze-out conditions in heavy ion collisions at  $\sqrt{s_{NN}} = 2.76$  TeV. *Phys. Rev. C* **90**, 054907 (2014). doi:[10.1103/PhysRevC.90.054907](https://doi.org/10.1103/PhysRevC.90.054907)

Modification of K0s and Lambda(AntiLambda)  
Transverse Momentum Spectra in Pb-Pb Collisions at  
 $\sqrt{s_{NN}} = 2.76$  TeV with ALICE

Schuchmann, S.

2016, XV, 207 p. 204 illus., 109 illus. in color.,

Hardcover

ISBN: 978-3-319-43457-5